Bulk, Spectral and Deep-Water Approximations for Stokes Drift: Implications for Coupled Ocean Circulation and Surface Wave Models

Guoqiang Liu,[1,2,3,4] Nirnimesh Kumar,[5] Ramsey Harcourt[6], and William Perrie[3,4]

Corresponding author: Guoqiang Liu, Bedford Institute of Oceanography, Fisheries and Oceans Canada, Dartmouth, NS, Canada. (Guoqiang.Liu@dfo-mpo.gc.ca)

[1]School of Marine Sciences, Nanjing

Abstract.

Surface waves modify upper ocean dynamics through Stokes drift related processes. Representation of these processes at either resolved or parameterized scales in an ocean model depends on accurate estimation of Stokes drift profiles. Stokes drift estimated from a discrete wave spectrum is com-

University of Information Science and Technology, Nanjing, Jiangsu, China

[2]Southern Marine Science and Engineering Guangdong Laboratory, Zhuhai, Guangdong, China

[3]Department of Engineering Mathematics and Internetworking Dalhousie University, Halifax, Nova Scotia, Canada

[4]Bedford Institute of Oceanography,Fisheries and Oceans Canada, Dartmouth, NS, Canada

[5]Department of Civil Environmental and Engineering, University of Washington, Seattle, WA, USA

[6]Applied Physics Laboratory, University of Washington, Seattle, WA, USA

pared to Stokes drift approximations as a monochromatic profile based on bulk surface wave parameters, and to two additional super-exponential functional forms. The impact of these different methods on resolved-scale ocean processes is examined in the context of two test-bed cases of a wave-current coupled system: (1) a shallow water inlet test case and (2) an idealized deep water hurricane case. In case (1), tidal currents can modify the waves and significantly affect Stokes drift computed from the wave spectrum. In both cases, large deviations in ocean current response are produced when the Stokes drift is approximated monochromatically from bulk wave parameters, rather than from integration over the wave spectra. Deep water simulations using the two super-exponential approximations are in better agreement with those estimated from wave spectra than are those using the monochromatic, exponential profile based on bulk wave parameters. In order to represent the impact of Stokes drift at resolved scales, we recommend that for studies of nearshore processes and brief deep water events, like wave-current interactions under storms, the Stokes drift should be calculated from full wave spectra. For long simulations of open ocean dynamics, methods using super-exponential profiles to represent equilibrium wind seas might be sufficient, but appear to be marginally more computationally efficient.

Plain Language Summary

The surface wave could induce a net drift in the direction of the wave propagation, known as the Stokes drift. It impacts the Lagrangian trajectories of floating matter over the ocean surface and plays an essential role in the

upper ocean mixing and the interaction between the surface wave and upper ocean processes. All these processes need an accurate estimation of Stokes drift profiles. The focus of this study is the implementation and validation of alternative and better methods to estimate the Stokes drift profiles in a coupled model system. We introduce a method that accounts for the complete frequency-directional spectrum, and two other approximate methods for applications in deep waters. The implementation of these methods in the coupled model creates new opportunities to explore the roles of processes driven by Stokes drift in parameterized mixing processes.

1. Introduction

The periodic, orbital motions of progressive surface gravity waves induce a net drift in the direction of wave propagation, known as the Stokes drift $\mathbf{u}^{\mathrm{St}}$. Formally, this drift motion is the difference between the phase-averaged Eulerian velocity and the mean Lagrangian motion of a particle in the wave field [*Stokes*, 1847]. In practice, the Stokes drift is approximated to lowest nontrivial order in the Taylor expansion of a Lagrangian trajectory, averaged over the phase of the wave. For a monochromatic progressive wave of amplitude A, radial frequency $\sigma = 2\pi f$ and wavenumber k in water of depth h, this approximation gives a profile over depth z (positive-up) of

$$u^{\mathrm{St}}(z) = A^2\sigma k \frac{\cosh(2k(z+h))}{2\sinh^2 kh}, \tag{1}$$

in the direction of propagation, and that simplifies to $u^{\mathrm{St}}(z) = A^2\sigma k \exp 2kz$ in the limit of deep water $kh \gg 1$. Stokes drift $\mathbf{u}^{\mathrm{St}}$ plays an important role for multiple processes in the marine environment: It accounts for around two-thirds of the wind-induced drift near the surface layer [*Rascle et al.*, 2008]; it is strongly sheared in the vertical direction [*Webb and Fox-Kemper*, 2011; *Breivik et al.*, 2014]; and it essentially determines the trajectories of drifting objects, buoyant pollutants and other substances over the ocean surface [*McWilliams and Sullivan*, 2000; *Breivik et al.*, 2012; *Röhrs et al.*, 2012, 2015]. Mass-flux induced by Stokes drift is conserved and leads to offshore-directed undertow in the surf zone and the inner-shelf [*Faria et al.*, 2000; *Lentz et al.*, 2008; *Kumar and Feddersen*, 2017], combined with momentum deposited by wave breaking [*e.g.*, *Deike et al.*, 2017]. Furthermore, Stokes drift modifies submesoscale fronts and filaments in the upper ocean [*McWilliams and Fox-Kemper*, 2013; *Suzuki et al.*, 2016; *McWilliams*, 2018].

The interaction between Stokes drift and the mean Eulerian current shear results in the Craik-Leibovich vortex force [*Craik and Leibovich*, 1976] that drives instabilities and generates Langmuir turbulence, which is a principal turbulent upper ocean process that controls mixing and turbulent transport in the ocean surface boundary layer [*Thorpe*, 2004; *Harcourt and D'Asaro*, 2008; *Sullivan and McWilliams*, 2010; *D'Asaro et al.*, 2014]. Coriolis force acting on surface wave velocities leads to an additional force referred to as the Stokes-Coriolis force or the Hasselmann wave stress [*Ursell and Deacon*, 1950; *Hasselmann*, 1970; *Polton et al.*, 2005], which modifies the mean current profile and alters the distribution of momentum in the upper ocean (*i.e.,* the Ekman profile) over both the open ocean and the coastal inner shelf [*McWilliams and Restrepo*, 1999; *Polton et al.*, 2005; *Lentz et al.*, 2008].

Directional wave buoys at specific locations in the continental shelf and coastal areas measure the directional buoy moments [*Longuet-Higgins et al.*, 1963], which can be used to estimate the complete frequency-directional wave spectrum $E(f, \theta)$ and thus the Stokes drift [*Kenyon*, 1969]. However, the spatial distribution of buoys is typically insufficient to estimate the Stokes drift profiles over domains of oceanographic interest, ranging from coastal regions up to the global ocean [*Webb and Fox-Kemper*, 2015; *Kumar et al.*, 2017; *van den Bremer and Breivik*, 2018; *Crosby et al.*, 2019]. Scatterometer observations can be used to estimate the surface Stokes drift [*e.g., Liu et al.*, 2014], however, this method does not provide the vertical distribution. Presently, the full water column Stokes drift is often estimated from the spectrum of a numerical wave model, an approach widely used in estimating the waves' Lagrangian transport [*Ardhuin et al.*, 2009; *Kumar et al.*, 2017]. Multiple coupled ocean and wave modeling systems exist, which quantify the surface wave effects on the upper ocean via Stokes drift [*Ardhuin et al.*, 2008; *Uchiyama et al.*, 2010a; *Warner et al.*, 2010; *Bennis et al.*, 2011; *Kumar et al.*, 2012; *Moghimi et al.*, 2013]. One of the widely used open-source codes is the Coupled Ocean-Atmosphere-Wave-Sediment Transport (COAWST) modeling system [*Warner et al.*, 2008, 2010], which tightly couples currents simulated in the Regional Ocean Model System [ROMS, *Shchepetkin and McWilliams*, 2005] to surface wave spectra in the Simulating Waves Nearshore [SWAN, *Booij et al.*, 1999] model. The interaction between surface waves and ocean circulation incorporates the Vortex-Force method [*McWilliams et al.*, 2004; *Uchiyama et al.*, 2010a; *Kumar et al.*, 2012]. This coupled modeling system has been extensively applied to nearshore and inner shelf studies, where the surface wave effects are important [*e.g., Kumar et al.*, 2012, 2015; *Olabarrieta et al.*, 2011; *Akan et al.*, 2017; *Moghimi et al.*, 2019]. Moreover, COAWST has also been used for short-term hurricane studies where intense surface wave activity leads to momentum and enthalpy flux exchanges at the air-sea interface [*Olabarrieta et al.*, 2012; *Zambon et al.*, 2014; *Reichl et al.*, 2016a, b; *Curcic et al.*, 2016]. These large surface waves also significantly modify the Lagrangian trajectories and upper ocean mixing via Stokes drift and Langmuir turbulence.

The representation of Langmuir turbulence in a turbulent mixing parameterization model, [*e.g., Harcourt*, 2013, 2015; *Wu et al.*, 2015; *Reichl et al.*, 2016a; *Li and Fox-Kemper*, 2017], the application of the Stokes-Coriolis force, or the inclusion of the vortex force in the momentum equations at resolved scales [*Kumar et al.*, 2012], all require an accurate representation of the Stokes drift velocity or its vertical shear [*van den Bremer and Breivik*, 2018]. However, computation of the Stokes drift profile from $E(f, \theta)$ is potentially numerically expensive, requiring a discrete integration over the wave spectrum at every depth level [*Kenyon*, 1969], and, in the absence of direct coupling to a wave model, at least cumbersome to store and apply as a forcing field. To reduce computational and data-transfer or storage expenses, the Stokes drift profile has often been estimated by a simplified expression, *e.g.,* as a monochromatic wave based on local bulk wave parameters (*i.e.,* significant wave height and mean wavelength and direction) in a wave-current coupled model, as in the existing ROMS-SWAN coupling within COAWST [*Kumar et al.*, 2012], as well as in other variants of ROMS [*Uchiyama et al.*, 2010a; *Marchesiello et al.*, 2015].

Nevertheless, representation of Stokes drift by a single monochromatic wave formulation is problematic and may introduce serious errors as: (a) The Stokes drift associated with short waves decays rapidly with depth, and so entails locally stronger Stokes shear and near-surface wave-current coupling than that associated with a monochromatic wave at an intermediate wavenumber corresponding to the mean wavelength; (b) The Stokes drift profile for a complete frequency-directional spectrum also becomes stronger at depth than for a monochromatic wave approximation, as the low-wavenumber components of the spectrum (*e.g.,* swell) penetrate much deeper [*Kenyon*, 1969; *Harcourt and D'Asaro*, 2008; *Breivik et al.*, 2016; *Webb and Fox-Kemper*, 2015]; and finally (c) in presence of multi-directional waves, a monochromatic Stokes drift estimate leads to inaccuracies in both magnitude and direction, thus impacting the associated Lagrangian transport [*Kumar et al.*, 2017]. In order to more accurately simulate the physical processes associated with Stokes drift, it is best to be calculated from the frequency-directional wave spectrum $E(f, \theta)$ before entering the equations for wave-averaged momentum and tracer equations in an Eulerian ocean model like ROMS, and ultimately before using it as forcing in any Langmuir turbulence mixing parameterization, as well.

Given the deficiencies associated with estimating Stokes drift using bulk wave parameters, multiple previous studies have identified alternate approaches for calculating $\mathbf{u}^{\mathrm{St}}$ by accounting for some aspect of the frequency-directional wave spectrum. Two methods have been proposed to approximate the super-exponential Stokes drift profiles generated by full integration over the spectrum $E(f, \theta)$ in deep water. *Breivik et al.* [2014] suggested estimation of Stokes drift by using a modified exponential profile of a monochromatic wave, and in a subsequent study [*Breivik et al.*, 2016] identified closed form solutions for Stokes drift by integrating the Philips spectrum assuming that it provides a reasonable estimate of the intermediate to high-frequency part of the real frequency-directional spectrum.

The present work focuses on evaluating the improvements effected in coupled modeling by replacing the monochromatic estimation of Stokes drift with discrete integration over the wave-model SWAN spectra $E(f, \theta)$ in the context of either deep or shallow water, and the relative benefits afforded by the two super-exponential approximations, where valid in a deep water case. Estimated Stokes drift profiles from all four approaches are implemented and compared in the context of a longstanding deep water ROMS test case for an idealized hurricane, which leads to complex wave conditions. For the shallow water context where valid super-exponential approximations have not yet been proposed, monochromatic estimates are compared with spectrally integrated Stokes drift forcing for a coastal inlet test case, with tidal forcing and offshore swell. Here, the relative importance of two-way coupling (*i.e.,* two-way exchange between the ocean circulation and the wave propagation model) in the evolution of $E(f, \theta)$ and subsequently the Stokes drift is also explored.

The outline for this paper is as follows: In section 2, the multiple methodologies for estimating Stokes drift profiles are presented. Section 3 describes the setup of the two test cases for shallow and deep water. Section 4 focuses on the Stokes drift profile and wave spectra simulated in the shallow water inlet test case, while section 5 demonstrates the variability of Stokes drift and vortex force in a hurricane, due to differences in Stokes drift formulations. Findings from this work are summarized in section 6.

2. Methods

2.1. Wave Effects on Currents (WEC) through Stokes Drift

The open-source COAWST modeling system [*Warner et al.*, 2010] v3.0 used in the present study couples the surface wave model SWAN to the ocean circulation model ROMS. SWAN simulates wave generation, dissipation, wave-wave interactions, shoaling, refraction, and depth-limited breaking processes [*Booij et al.*, 2004]. ROMS is a three dimensional ocean circulation model solving the wave-averaged Navier-Stokes equations with hydrostatic and Boussinesq approximations. The wave-current interactions in COAWST used here are based on the vortex force formalism [*McWilliams et al.*, 2004], separating conservative and non-conservative wave effects [wave breaking induced energy and momentum forcing, *Uchiyama et al.*, 2010a; *Kumar et al.*, 2012]. The Stokes drift is used to estimate the surface Lagrangian trajectories, Stokes-Coriolis force, the vortex force and the associated Bernoulli head.

The ROMS model uses an orthogonal curvilinear grid in the horizontal and a stretched terrain following vertical s-coordinate system. Here, simplified momentum balance components in Cartesian coordinates $(x,\, y)$ are presented to identify the terms dependent on the Stokes drift and wave-current interaction. The x-component of momentum is,

$$\begin{aligned}
&\frac{\partial}{\partial t}\left(H_z^c u\right) + \underbrace{\frac{\partial}{\partial x}\left(H_z^c u^2\right) + \frac{\partial}{\partial y}\left(H_z^c uv\right) + u\frac{\partial}{\partial x}\left(H_z u^{\mathrm{St}}\right) + u\frac{\partial}{\partial y}\left(H_z v^{\mathrm{St}}\right)}_{1\, A_1^h} \\
&+\underbrace{\frac{\partial}{\partial s}\left(w_s u\right) + u\frac{\partial w_s^{\mathrm{St}}}{\partial s}}_{2\, B_1^h} = -H_z^c \left.\frac{\partial \varphi^c}{\partial x}\right|_z + H_z^c f v + \underbrace{H_z^c f v^{\mathrm{St}}}_{3\, C_1^s} + \underbrace{H_z^c v^{\mathrm{St}}\left(\frac{\partial v}{\partial x} - \frac{\partial u}{\partial y}\right)}_{4\, J_1^h} \underbrace{-w_s^{\mathrm{St}}\frac{\partial u}{\partial s}}_{5\, J_1^v} \qquad (2) \\
&+H_z^c F^x + H_z^c F^{wx} + H_z^c D^x - \frac{\partial}{\partial s}\left(\overline{u'w'} - \frac{v}{H_z^c}\frac{\partial u}{\partial s}\right)
\end{aligned}$$

y-component momentum,

$$\begin{aligned}
&\frac{\partial}{\partial t}\left(H_z^c v\right) + \underbrace{\frac{\partial}{\partial x}\left(H_z^c uv\right) + \frac{\partial}{\partial y}(H_z^c v^2) + v\frac{\partial}{\partial x}\left(H_z^c u^{\mathrm{St}}\right) + v\frac{\partial}{\partial y}\left(H_z^c v^{\mathrm{St}}\right)}_{1\, A_2^h} \\
&+\underbrace{\frac{\partial}{\partial s}\left(w_s v\right) + v\frac{\partial w_s^{\mathrm{St}}}{\partial s}}_{2\, B_2^h} = -H_z^c \left.\frac{\partial \varphi^c}{\partial y}\right|_z - H_z^c f u - \underbrace{H_z^c f u^{\mathrm{St}}}_{3\, C_2^s} \underbrace{-H_z^c u^{\mathrm{St}}\left(\frac{\partial v}{\partial x} - \frac{\partial u}{\partial y}\right)}_{4\, J_2^h} \underbrace{-w_s^{\mathrm{St}}\frac{\partial v}{\partial s}}_{5\, J_2^v} \qquad (3) \\
&+H_z^c F^y + H_z^c F^{wy} + H_z^c D^y - \frac{\partial}{\partial s}\left(\overline{v'w'} - \frac{v}{H_z^c}\frac{\partial v}{\partial s}\right),
\end{aligned}$$

and the continuity equation,

$$\frac{\partial H_z^c}{\partial t} + \frac{\partial}{\partial x}\left(H_z^c\left(u + u^{\mathrm{St}}\right)\right) + \frac{\partial}{\partial y}\left(H_z^c(v + v^{\mathrm{St}})\right) + \frac{\partial}{\partial s}\left(w + w^{\mathrm{St}}\right) \;=\; 0 \qquad (4)$$

where u, v, w are the quasi-Eulerian mean velocities, defined as the Lagrangian mean velocity minus the Stokes drift $u^{\mathrm{St}}, v^{\mathrm{St}}, w^{\mathrm{St}}$. Here, f is the Coriolis parameter, φ is the dynamic pressure (normalized by the density ρ_0), F^x and F^y are non-wave, non-conservative forces, D^x and D^y represent the horizontal diffusive terms, F^{wx} and F^{wy} are the sum of the momentum flux due to all non-conservative wave induced forces (*e.g.,* wave breaking and roller-induced acceleration), and H_z^c is the grid cell thickness. The overbar and prime indicate the time average and turbulent fluctuating quantity, respectively, and ν is the molecular viscosity. To simplify the presentation of more complex ROMS equations, the Lamé metric coefficients are assumed to be unity, and additional terms corresponding to the curvilinear grid are not included. The turbulent parts $[\overline{u'w'}, \overline{v'w'}]$ are parameterized by using a turbulence-closure model. In this study, we use the $k-\epsilon$ generic length-scale (GLS) method [*Umlauf and Burchard*, 2003; *Warner et al.*, 2005], a turbulence closure that does not yet incorporate forcing of Langmuir turbulence by the Stokes drift.

The momentum and mass conservation equations for the ROMS-SWAN coupled system show the effect of surface gravity waves manifested through Stokes drift on Eulerian mean flows in the terms for horizontal and vertical advection (①$A_1^h; A_2^h$, ②$B_1^h; B_2^h$); Stokes-Coriolis forces (③$C_1^s; C_2^s$), horizontal and vertical vortex forces (④$J_1^h; J_2^h$, ⑤$J_1^v; J_2^v$) and Stokes drift divergence (Eqn. 4). Furthermore, the three dimensional wave-averaged equations are not only dependent on the surface Stokes drift but also its vertical profile, which has implications for wave-induced mass fluxes and nearshore circulation [*Uchiyama et al.*, 2010a; *Kumar et al.*, 2012, 2013].

2.2. Stokes Drift Representations

2.2.1. Representation from a Broadband Frequency-Directional Spectrum

Accurate representation of the Stokes drift requires a spectral approach. The Stokes drift in water of arbitrary depth can be estimated by a linear superposition of contributions from the complete frequency-directional wave energy spectrum $E(\sigma,\theta)$ as

$$\mathbf{u}^{\mathrm{St}}(z) = 2\int_0^{2\pi}\int_0^{\infty} \sigma\mathbf{k}E(\sigma,\theta)\,\frac{\cosh\left[2k(z+h)\right]}{2\sinh^2(kh)}d\sigma d\theta, \tag{5}$$

where θ is the wave direction, $\mathbf{k}$ is the vector wavenumber [*Phillips*, 1966; *Kenyon*, 1969], and $\sigma = 2\pi f$ is the radial frequency. In the deep-water limit of the dispersion relation,

$\sigma^2 = gk$, Eqn. 5 simplifies to

$$\mathbf{u}^{\mathrm{St}}(z) = \frac{2}{g} \int_0^{2\pi} \int_0^{\infty} \sigma^3 \widehat{\mathbf{k}} E(\sigma,\theta)\, e^{2kz} d\sigma d\theta, \tag{6}$$

where $\widehat{\mathbf{k}} = \mathbf{k}/|k|$. As shown in Eqn. 5, computing Stokes drift profiles from a full frequency directional wave spectrum involves integration over direction, and over frequency at each vertical level, and depends upon the third moment of the vertically attenuated wave spectrum. Shorter, higher frequency components may contribute significantly to near-surface Stokes shear and surface Stokes drift, but these decay rapidly with depth. Net transport by the Stokes drift is related to the first moment of the frequency spectrum.

2.2.2. Representation by a monochromatic exponential profile

Over recent decades, studies focused on wave-current interaction or on small-scale Craik-Leibovich interactions of Langmuir turbulence [*McWilliams et al.*, 1997] have often used an idealized monochromatic representation of ocean waves at a single frequency. This simplification restricts the Stokes drift representation accuracy to only a few independent features of the profile. For example, in the existing version of COAWST, the Stokes drift $\mathbf{u}^{\mathrm{St}}(z)$ is estimated from wave energy E_w (per unit density and area), and the celerity c of the spectrally-weighted mean wavenumber $\overline{k}$, to have a surface value of $2E_w\overline{k}/c$, oriented in the mean direction of energy propagation, and to decay with depth as in Eqn. 1 for wavenumber $\overline{k}$. As mentioned earlier, this approach has multiple deficiencies in estimation of the surface Stokes drift, the Stokes drift transport, and other associated quantities. In the context of the deep water approximation, the surface value is underestimated by effectively replacing the third moment of the frequency spectrum by the 3/2-power of the second moment, and by replacing the super-exponential shape produced by the appropriately weighted average of exponential decays e^{2kz} of spectral elements, with the vertical decay for the mean wavenumber $e^{2\overline{k}z}$.

2.2.3. Representation by Super-Exponential Functions

Super-exponential functions can provide an improved match over monochromatic approximations to dynamically important properties of the Stokes drift profile due to broadband wind sea spectra. Several such formulations have been proposed, in order to retain the mathematical and numerical simplicity of representing the shape of the Stokes drift profile by a single function in closed form, and to do so efficiently under the assumption of equilibrium wind seas when detailed wave spectra are unavailable. *Breivik et al.* [2014] proposed an approximation for the super-exponential Stokes drift profiles of equilibrium wind-sea spectra in deep water based on re-scaling the exponential profile of a monochromatic wave [*McWilliams and Sullivan*, 2000; *Polton et al.*, 2005; *Saetra et al.*, 2007; *Tamura et al.*, 2012]. This formulation is denoted as the exponential integral profile (EIP), whereby the surface Stokes drift and Stokes transport are represented as:

$$\left|\mathbf{u}_{\mathrm{Tran}}^{\mathrm{St}}\left(z\right)\right| = \left|\mathbf{u}^{\mathrm{St}}\left(0\right)\right| \frac{e^{2k_e z}}{1 - Ck_e z} \tag{7}$$

where

$$k_e = \frac{\left|\mathbf{u}^{\mathrm{St}}\left(0\right)\right|}{5.97\left|\mathbf{T}_{\mathrm{s}}\right|}. \tag{8}$$

Here $\mathbf{u}^{\mathrm{St}}(0)$ is the surface Stokes drift vector, the constant coefficient $C \approx 8$, and $\mathbf{T}_{\mathrm{s}}$ is the Stokes transport vector, estimated as

$$\mathbf{T}_{\mathrm{s}} = \int_0^{2\pi}\int_0^{\infty} \sigma^2 \widehat{\boldsymbol{k}} N\left(\sigma,\theta\right) d\sigma d\theta. \tag{9}$$

The EIP based Stokes drift profile (Eqn. 7) is a better approximation than the monochromatic wave profile estimate (Eqn. 1), with a 60% reduction in root-mean-square error

[*Breivik et al.*, 2014]. However, the Stokes drift shear estimated by EIP is weak at the order of Stokes depth scale, $(= 1/2k)$, as the near-surface Stokes shear is determined mostly by the intermediate-to-high frequency part of the wave spectrum.

A second alternate formulation to represent Stokes drift was also developed by assuming that the Philips spectrum, with $E(\sigma) \sim \sigma^{-5}$, is a good representation for the intermediate to high frequency portion of the wave spectrum for fully-developed local wind seas [*Phillips*, 1958, 1985; *Janssen*, 2004]. This new Stokes drift profile proposed by *Breivik et al.* [2016] is given by,

$$\mathbf{u}^{\mathrm{St}}_{\mathrm{Phil}}(z) = \mathbf{u}^{\mathrm{St}}(0)\left[e^{2k_p z} - \beta\sqrt{-2k_p \pi z}\,\mathrm{erfc}\left(\sqrt{-2k_p z}\right)\right]. \tag{10}$$

The peak wavenumber k_p is set equal to the inverse depth scale k_d, estimated as

$$k_d \approx \frac{\left|\mathbf{u}^{\mathrm{St}}(0)\right|}{2\left|\mathbf{T}_{\mathrm{s}}\right|}(1 - 2\beta/3), \tag{11}$$

and erfc is the complementary error function. Here, as in *Breivik et al.* [2016], the constant $\beta = 1$ is used to calculate k_d.

2.2.4. Stokes drift Contribution from a High-frequency Tail

In order to make comparisons between the super-exponential representations and Stokes drift computed by discrete integration over wave model frequencies limited by the cut-off in resolution at σ_c, it becomes necessary to estimate the contribution from above the cut-off by attaching a high-frequency tail to the resolved spectrum. As Stokes drift is weighted toward the high-frequency (HF) part of the wave spectrum, the tail beyond the highest resolved σ_c in the wave model can be a significant fraction of the surface value $\mathbf{u}^{\mathrm{St}}(0)$ and the near-surface profile. In SWAN, the cut-off frequency is always the same as the maximum frequency. The impact of the tail on ocean dynamics will therefore be a strong function of the choice for frequency cut-off. Therefore, for reasons of numerical expediency, in cases where the cutoff frequency is low, including an estimated contribution from the tail can always be expected to be more physically correct than omitting this contribution would be, and can be expected to have a significant impact. Here, we assume that the HF tail contribution falls entirely within the deep-water regime and has the form

$$\mathrm{E}_{\mathrm{HF}}\left(\sigma,\theta\right) = \mathrm{E}\left(\sigma_c,\theta\right)\left(\sigma_c/\sigma\right)^5, \tag{12}$$

consistent with the Philips spectrum. The additional Stokes drift from the high-frequency tail is

$$\mathbf{u}_{\mathrm{HF}}^{\mathrm{St}}\left(z\right) = \frac{2\sigma_c^5}{g}\int_0^{2\pi}\mathrm{E}\left(\sigma_c,\theta\right)\widehat{\boldsymbol{k}}d\theta\int_{\sigma_c}^{\infty}\frac{\exp\left(2z\sigma^2/g\right)}{\sigma^2}d\sigma. \tag{13}$$

Using integral relations [*e.g., Gradshteyn and Ryzhik*, 2007],

$$\mathbf{u}_{\mathrm{HF}}^{\mathrm{St}}\left(z\right) = \frac{2\sigma_c^4}{g}\left[\exp\left(-\mu\sigma_c^2\right) - \sigma_c\sqrt{\mu\pi}\,erfc\left(\sigma_c\sqrt{\mu}\right)\right]\int_0^{2\pi}E\left(\sigma_c,\theta\right)\widehat{\boldsymbol{k}}d\theta \tag{14}$$

where $\mu = -2z/g$. Note this is equivalent to $\mathbf{u}_{\mathrm{Phil}}^{\mathrm{St}}$ setting $k_p = \sigma_c^2/g$ with surface Stokes drift

$$\mathbf{u}_{\mathrm{HF}}^{\mathrm{St}}\left(0\right) = \frac{2\sigma_c^4}{g}\int_0^{2\pi}\mathrm{E}\left(\sigma_c,\theta\right)\widehat{\boldsymbol{k}}d\theta, \tag{15}$$

i.e., σ_c times the spectral density of Stokes drift at the cut-off. Transport by the tail is

$$\mathbf{T}_{\mathrm{HF}}^{\mathrm{St}} = \frac{\sigma_c^2}{3}\int_0^{2\pi}\mathrm{E}\left(\sigma_c,\theta\right)\widehat{\boldsymbol{k}}d\theta. \tag{16}$$

A detailed analysis of the accuracy of SWAN predictions at the cut-off frequency and tail-contribution is quite beyond the scope of this project. However, we anticipate to learn of the accuracy of these formulations through applications, rather than simply omitting the tail contributions.

2.3. Implementation of Stokes Drift in COAWST

2.3.1. Exponential Stokes Drift Profile with Bulk Methods

In the existing version of COAWST, the wavelength $L_w = 2\pi/\overline{k}$ of the mean wavenumber $\overline{k}$, the mean direction θ_m of energy propagation, and the significant wave height H_s are calculated within SWAN from the action density spectrum $N(\sigma, \theta) = E(\sigma, \theta)/\sigma$, generally used as the prognostic variable in numerical wave models. After passing these two bulk variables to ROMS through the Model Coupling Toolkit (MCT) coupler, wave energy $\mathrm{E}_w = gH_\mathrm{s}^2/16$ and the wavenumber $\overline{\boldsymbol{k}} = \overline{k}cos(\theta_m))\widehat{\boldsymbol{i}} + \overline{k}sin(\theta_m))\widehat{\boldsymbol{j}}$ are determined from H_s, L_w and θ_m. The monochromatic exponential profile of Stokes drift $\mathbf{u}^{\mathrm{St}}(z)$ (Eqn. 1) is computed as a depth-average over the local vertical grid layer [*Harcourt and D'Asaro*, 2008], which varies with water depth and surface elevation within ROMS as

$$\mathbf{u}_{\mathrm{B}}^{\mathrm{St}}(z) = \frac{2E_w\sigma\overline{\boldsymbol{k}}}{g}\frac{\sinh(k\Delta z)}{k\Delta z}\frac{\cosh(2k(z+h))}{2\sinh^2 kh}, \tag{17}$$

and in the deep water limit,

$$\mathbf{u}_{\mathrm{B}}^{\mathrm{St}}(z) = \frac{2E_w\overline{\boldsymbol{k}}}{c}\frac{\sinh(k\Delta z)}{k\Delta z}e^{2kz}. \tag{18}$$

The additional factor of $\sinh(k\Delta z))/k\Delta z$ accounts for integration over the grid layer of thickness Δz, with or without the deep-water approximation. Here the subscript B indicates estimates using bulk formulations. This modification of the strictly exponential form (Eqn. 1) avoids producing artificial convergences in horizontal Stokes drift and transport, and makes the depth-integrated transport and the forcing terms in Eqn. 2, 3 insensitive to changes in vertical resolution. However, layer-averaging is not without drawbacks, as it does artificially shift the profile of Stokes shear downwards near the surface.

2.3.2. Spectral method for Stokes Drift Profile

The COAWST modeling system has been modified to calculate the Stokes drift profiles in ROMS based on integration over the complete directional wave spectrum (*i.e.*, Eqn. 5). For efficient discrete integration over $N_\sigma \times N_\theta$ frequency-directional spectral contributions and the transfer from SWAN to the depth-dependent Stokes drift in ROMS, the spectrum of the Stokes drift $\mathbf{u}_{\rm ss}(\sigma)$ is first computed by radial integration

$$\mathbf{u}_{\rm ss}(\sigma) = 2\sum_{1}^{N_\theta} \sigma^2 N\left(\sigma,\theta\right) \boldsymbol{k}\Delta\theta \tag{19}$$

within SWAN. The two 1-dimensional components of the Stokes spectrum are then transferred to ROMS via the MCT coupling as three arrays, consisting of the Stokes drift

$$\left[\hat{\mathbf{u}}_{\rm ss}\Delta\sigma\right]_i = \frac{\left(\mathbf{u}_{\rm ss}(\sigma_i) + \mathbf{u}_{\rm ss}(\sigma_{i+1})\right)\left(\sigma_{i+1} - \sigma_i\right)}{2} \tag{20}$$

attributable to each frequency interval, and the corresponding array of $N_{\sigma-1}$ average wavenumbers $\check{k} = (k_i + k_{i+1})/2$. To transfer the multiple arrays at each coupling point, the existing model coupler routines within COAWST (for defining and effecting scalar transfers) are invoked iteratively.

Within ROMS, the Stokes drift profile is subsequently computed as grid layer averages, as is done for the monochromatic profile (Eqn. 17), at the depths where ROMS horizontal velocities are evaluated. The shallow water formulation is applied only to the N_{sw} frequencies with $\check{k}h < 18$, with the deep water formulation applied at higher frequencies, and supplemented by a grid-averaged high-frequency Stokes drift contribution $\mathbf{u}_{\rm HF}^{\rm St}$ from the spectral tail:

$$\begin{aligned}\mathbf{u}_{\rm S}^{\rm St}(z) = &\sum_{1}^{N_{sw}} \frac{\cosh(2\check{k}(z+h))}{2\sinh^2\check{k}h}\frac{\sinh(\check{k}\Delta z)}{\check{k}\Delta z}\hat{\mathbf{u}}_{\rm ss}\Delta\sigma \\ &+ \sum_{N_{sw}+1}^{N_\sigma - 1}\frac{\sinh(\check{k}\Delta z)}{\check{k}\Delta z}e^{2\check{k}z}\hat{\mathbf{u}}_{\rm ss}\Delta\sigma + \mathbf{u}_{\rm HF}^{\rm St}.\end{aligned} \tag{21}$$

Here the subscript S, refers to estimates of Stokes drift using spectral formulations. The discrete integrals over $\sigma < \sigma_c$ are computed trapezoidally using $\check{k}$ and $\hat{\mathbf{u}}_{\mathrm{ss}}$. The error introduced by approximating Stokes drift from higher frequencies using the deep-water approximation in the second integral is limited to $\mathcal{O}(10^{-15})$ times the sum over the magnitude of surface contributions $|\mathbf{u}_{\mathrm{ss}}(\sigma)|\,\Delta\sigma$. Moreover, contributions from $-\check{k}z > 36$ are omitted from the sum entirely to reduce the computational load from depths where the Stokes drift is insignificant.

The surface value $\mathbf{u}^{\mathrm{St}}_{\mathrm{HF}}(0) = \sigma_c \mathbf{u}_{\mathrm{ss}}(\sigma_c)$ of the tail contribution (Eqn. 15) is computed in SWAN assuming the deep-water approximation and a Phillips spectrum for $\sigma > \sigma_c$, and passed via the MCT, with the cut-off wavenumber k_c as terminal elements of the three arrays of $\hat{\mathbf{u}}_{\mathrm{ss}}\Delta\sigma$ and $\check{k}$. The contribution to the grid-layer averaged Stokes drift profile is then computed as in [*Harcourt and D'Asaro*, 2008]:

$$\mathbf{u}^{\mathrm{St}}_{\mathrm{HF}}(z) = \frac{\mathbf{u}^{\mathrm{St}}_{\mathrm{HF}}(0)}{2k_c\Delta z}[a_- I(a_-)) - a_+ I(a_+))], \tag{22}$$

where

$$I(a_\pm) = \frac{2}{3}\left[\sqrt{a_\pm \pi}\,\mathrm{erfc}(a_\pm^{1/2}) - \left(1 - \frac{1}{2a}\right)e^{-a}\right], \tag{23}$$

where $a_\pm = -2(z \pm \frac{\Delta z}{2})k_c$. This expression for the layer average tail contribution assumes that the deep water dispersion relation and Stokes drift formulations apply at and above the cutoff wavenumber σ_c^2/g. It is computed in the top ROMS grid layer, but below that only where $-k_c z < 36$.

2.3.3. Implementation of Super-exponential functions

For purposes of comparison between super-exponential forms and the spectrally integrated $u^{\mathrm{St}}_{\mathrm{S}}$, tail contributions to surface Stokes drift and transport (Eqns. 15,16) are computed within SWAN and passed to ROMS, where they are included in evaluating the closed-form expressions (Eqns. 7-11) for $u^{\mathrm{St}}_{\mathrm{Tran}}$ and $u^{\mathrm{St}}_{\mathrm{Phil}}$. Note that substitution of peak k_p, σ_p and $\mathbf{u}^{\mathrm{St}}(0)$ from a Phillips spectrum for k_c, σ_c in $\mathbf{u}^{\mathrm{St}}_{\mathrm{HF}}$ in Eqns. (21,22) may be used to determine the grid-layer averaged profile of $\mathbf{u}^{\mathrm{St}}_{\mathrm{Phil}}$, a forcing variant not evaluated here. Fig. 1 shows the flowchart for the four methods of calculating Stokes drift, $u^{\mathrm{St}}_{\mathrm{B}}$, $u^{\mathrm{St}}_{\mathrm{Tran}}$, $u^{\mathrm{St}}_{\mathrm{Phil}}$ and $u^{\mathrm{St}}_{\mathrm{S}}$, showing the equations used for each method and the associated variables that are transferred from SWAN to ROMS.

2.3.4. Inter-comparison between Stokes Drift Estimates

Even though the approximations involved in estimating Stokes drift profile vary for the different formulations chosen here (*i.e.,* Eqns. 7, 10, 17, 21), the surface Stokes drift (*i.e.,* at $z = 0$) is expected to be same from Eqns. 7, 10, and 21, while estimates from Eqn. 17 are expected to differ as the bulk formulation does not account for any off-wind directional characteristics [*Kumar et al.*, 2017]. Yet, in the cases discussed here using the ocean circulation model ROMS, the near-surface estimates of Stokes drift are still not expected to match, as this average over the top grid layer $\mathbf{u}^{\mathrm{St}}$ is not at $z = 0$. Instead, ROMS follows an Arakawa C-grid configuration such that the velocities are defined at the vertical center of the grid cells, which is shifted slightly below the surface. Furthermore, the surface in ROMS is defined by the mean sea-surface elevation η, which varies between simulations, thus leading to small differences in the respective grid cell centers. Therefore, the first layer of $\mathbf{u}^{\mathrm{St}}$ location, is slightly below the real sea surface, leading to different estimates from these approximations.

3. Experiment Design

In this study COAWST with multiple implementations of Stokes drift is applied to study wave-current interaction dynamics in a tidal inlet, and for waves generated due to hurricane winds. These test cases are chosen to demonstrate the relative importance of the choice of Stokes drift in shallow and deep-water applications, within an environment consisting of strong wave-current interaction.

3.1. Tidal inlet wave-current coupled system

The first test case used in this paper is a simplified tidal inlet system, which is often utilized to test the wave-current interactions for a shallow water environment [*Warner et al.*, 2008]. The numerical domain is a rectangular basin with width 15 km and length 14 km. With a constant slope of 1/640 and a maximum water depth of 14.7 meters along the northern boundary, the entire domain is initialized at a uniform water level that is 4 meters deep in the nearshore. The back barrier region (bottom, Fig. 2a) is enclosed with four walls, with a 2 km wide inlet centered along the middle wall that connects the back region to the seaward part of the domain. The northern, western, and eastern edges of the seaward region are open. The western and eastern boundaries are "coastal wall" boundary conditions. The model system is forced by an oscillating water level on the northern edge, with a tidal amplitude of 1 meter and a period of 12 hours. Waves are imposed on the northern edge with a significant wave height, $H_\mathrm{s} = 1$ m, directed to the south with a period of 10 seconds. The SWAN model uses twenty-five frequency bins (0.04-1 Hz) with a logarithmically distributed frequency resolution and thirty six directional bands with a directional resolution of 10°. The wave spectrum at the northern boundary is a JONSWAP spectrum, set by the aforementioned bulk wave parameters. The water level oscillations drive the ocean circulation model and the wave forcing drives the wave propagation model. The surface wave field can be significantly modified by wave refraction, from bathymetry and current variability. The model simulation is conducted for a period of 12 hours.

The detailed parameter choices for the tidal inlet case are listed in Table 1. In order to demonstrate the wave spectrum variation by refraction along with implications for Stokes drift, the coupled model simulations are conducted with two configurations: (1) one-way coupled with wave information passed to ROMS (R_1); (2) two-way coupled model with wave information passed to ROMS, and currents and sea-surface elevation provided to SWAN (R_2). In this latter configuration, the effective velocity estimated from *Kirby and Chen* [1989] are provided to SWAN. For both configurations, (1) and (2), Stokes drift was estimated using the standard bulk wave parameters ($u_{\mathrm{B}}^{\mathrm{St}}$, $v_{\mathrm{B}}^{\mathrm{St}}$) and complete directional spectra ($u_{\mathrm{S}}^{\mathrm{St}}$, $v_{\mathrm{S}}^{\mathrm{St}}$), thus leading to four model simulations for intercomparison.

In simulation R_1, the surface wave propagation is affected by the bathymetry variability only, while in R_2 the bathymetry, sea level and current variations modify the wave propagation. Since the deep water dispersion relation is applied for $u_{\mathrm{Tran}}^{\mathrm{St}}$ and $u_{\mathrm{Phil}}^{\mathrm{St}}$, both these methods ignore bathymetric effects on surface waves and thus on Stokes drift, and therefore are not applicable for the shallow water applications like the present test case.

3.2. Idealized Hurricane case

In order to further assess the effects of different formulations on Stokes drift estimates, the complex, rapidly changing wave spectra generated under idealized hurricane wind forcing are considered. Typically, the strong, intense seas occur on the right-hand forward side of a translating hurricane, while relatively low energy waves are on the left-hand side, and the relatively young, low seas occur on the backside [*Black et al.*, 2007]. In the idealized hurricane case, a large, deep water domain is constructed for both the ocean and the wave model, so that the surface waves do not feel the bottom. Since the domain boundary is far from the hurricane center, it does not affect the simulations of waves and currents under the hurricane forcing. The wind vectors are derived from an analytic model of the wind and pressure profiles in hurricanes [*Holland*, 1980]. Here, the central pressure is 950 hPa, the environmental pressure is 1013 hPa, maximum wind speed is $V_m = 50$ ms^{-1} , radius of maximum wind is $R_{mw} = 55$ km, and air density is $\rho_a = 1.28$ kgm^{-3}, which are typical for Atlantic hurricanes. The wind stress field follows the hurricane in propagating from south to north of the model domain with a specified speed of 5.7 ms^{-1}. Once the wind field is generated, the wind stress magnitude is calculated using the bulk formula, in which the drag coefficient (C_d) is calculated as an empirical function of the 10-m wind speed [*Zijlema et al.*, 2012]. Using the same frequency-directional grid as the inlet case, the open boundary for SWAN is provided by a JONSWAP spectrum, and it is assumed that waves generated inside the domain can leave the area freely. Heat fluxes associated with air-sea interface are neglected as they are not dynamically significant, relative to the wind stress forcing.

For ROMS, the bathymetry is set to a constant value of 4000 meters with no land boundary, and 32 levels in the vertical direction, with increased resolution achieved with vertical stretching and 7 grid cells in the upper 50 meters. The horizontal model grid has an average of 10 km resolution. All the experiments are simulated for a period of 24 hours, and in each case the ocean is initialized with a homogeneous salinity (S) (35 PSU), temperature (T) profiles and no background currents. The temperature profile is based on the World Ocean Atlas (WOA) 09 climatological data for the north subtropical Atlantic ocean during the month of September [*Levitus et al.*, 2002]. Since the wind stress field translates from south to north of the model domain with a specified speed of 5.7 ms^{-1}, a period of 24 hours is deemed sufficient for analyzing the modeled dynamics, which corresponds to the strong wave conditions simulated here. Four simulations are conducted for the hurricane case, corresponding to the four different formulations for the Stokes drift profiles. Considering that the focus of this study is to determine the role of different formulations to estimate the Stokes drift profile in the presence of hurricane-generated waves, we ignore the currents and sea level effects, which can be important [*Fan et al.*, 2009] and must be included in realistic simulations. Thus, only wave parameters from SWAN are sent to ROMS, while SWAN receives no information from ROMS.

3.3. Velocity Symbols and Conventions

The Stokes drift velocity vector estimated using bulk (Eqn. 17), spectral (Eqn. 21), and those using super-exponential profiles (Eqns. 7, 10 are referred to as $\mathbf{u}_{\mathrm{B}}^{\mathrm{St}}$, $\mathbf{u}_{\mathrm{S}}^{\mathrm{St}}$, $\mathbf{u}_{\mathrm{Tran}}^{\mathrm{St}}$ and $\mathbf{u}_{\mathrm{Phil}}^{\mathrm{St}}$, respectively. The scalar eastward (northward)/zonal (meridional) velocity components are referred to as $u_{\mathrm{B}}^{\mathrm{St}}$ ($v_{\mathrm{B}}^{\mathrm{St}}$), $u_{\mathrm{S}}^{\mathrm{St}}$ ($v_{\mathrm{S}}^{\mathrm{St}}$), $u_{\mathrm{Tran}}^{\mathrm{St}}$ ($v_{\mathrm{Tran}}^{\mathrm{St}}$), and $u_{\mathrm{Phil}}^{\mathrm{St}}$ ($v_{\mathrm{Phil}}^{\mathrm{St}}$). The Stokes drift velocity magnitude are represented as $U_{\mathrm{B}}^{\mathrm{St}}$, $U_{\mathrm{S}}^{\mathrm{St}}$, $U_{\mathrm{Tran}}^{\mathrm{St}}$ and $U_{\mathrm{Phil}}^{\mathrm{St}}$. For the shallow water tidal-inlet case, the Stokes drift velocity components are referred to as $u_{\mathrm{B1}}^{\mathrm{St}}$, $v_{\mathrm{B1}}^{\mathrm{St}}$ and $u_{\mathrm{S1}}^{\mathrm{St}}$, $v_{\mathrm{S1}}^{\mathrm{St}}$ for one-way coupled simulations, and $u_{\mathrm{B2}}^{\mathrm{St}}$, $v_{\mathrm{B2}}^{\mathrm{St}}$ and $u_{\mathrm{S2}}^{\mathrm{St}}$, $v_{\mathrm{S2}}^{\mathrm{St}}$ for two-way coupled simulations.

4. Shallow water Inlet Test Case

Wave-current interactions in the shallow water tidal inlet test case are analyzed 12 hours after initialization with one-way (R_1) and two-way (R_2) coupling. The last hourly output from the model simulation is analyzed and presented.

4.1. Significant Wave Height, H_s

For simulation R_1, the modeled H_s decreases from 1 m at the offshore boundary to 0.75 m at the tidal inlet. Subsequently, the significant wave height decreases further as waves propagate within the tidal inlet (Fig. 2a). Two-way coupling between ROMS and SWAN (*i.e.,* simulation R_2) allows for the transfer of near-surface currents and sea-surface elevation from ROMS (Fig. 2d), which substantially modifies the SWAN simulated H_s. Particularly for R_2, adjacent to the inlet, H_s increases to 1m (Fig. 2b), such that the difference between simulated H_s for two-way and one-way coupling is up to 0.20 m ($\approx 20\%$, Fig. 2c). These differences in H_s manifest themselves adjacent to the tidal inlet due to strong ebb tidal currents opposing wave propagation (Fig. 2d), leading to local refraction and wave steepening.

4.2. Near-surface Stokes Drift

The choice of one-way versus two-way coupling also has implications for Stokes drift estimates. The near-surface eastward Stokes drift for R_1 estimated using bulk ($u^{\mathrm{St}}_{\mathrm{B1}}$) and spectral formulations ($u^{\mathrm{St}}_{\mathrm{S1}}$) at the topmost s layer (the ROMS vertical S-coordinate, which is a generalized vertical, terrain-following, coordinate system [*Shchepetkin and McWilliams*, 2005]) are compared in Fig. 3. Both $u^{\mathrm{St}}_{\mathrm{B1}}$ and $u^{\mathrm{St}}_{\mathrm{S1}}$ vary between ± 0.002 ms^{-1}, with strongest values around the tidal inlet (Fig. 3a,b). Differences between $u^{\mathrm{St}}_{\mathrm{B1}}$ and $u^{\mathrm{St}}_{\mathrm{S1}}$ are small ($\leq 5\%$), and are attributed to the small change in wave field due to bathymetric variability (Fig. 3c). For two-way coupled simulations, bathymetry, circulation pattern, and sea-surface elevation variability modify the surface wave propagation, which has implications for the Stokes drift profile. Adjacent to the tidal inlet, R_2 simulated near-surface $u^{\mathrm{St}}_{\mathrm{B2}}$ and $u^{\mathrm{St}}_{\mathrm{S2}}$ (*i.e.,* at the topmost s layer) are an order of magnitude larger than $u^{\mathrm{St}}_{\mathrm{B1}}$ and

$u^{\mathrm{St}}_{\mathrm{S1}}$ (compare Figs. 3a and 3d, Figs. 3b and 3e). Furthermore, for R_2 the difference between near-surface eastward Stokes drift estimates $u^{\mathrm{St}}_{\mathrm{S2}}$ and $u^{\mathrm{St}}_{\mathrm{B2}}$ are substantially larger than those determined for simulation R_1 (Figs. 3c and 3f).

Modeled northward near-surface Stokes drift from simulation R_1, $v^{\mathrm{St}}_{\mathrm{B1}}$ and $v^{\mathrm{St}}_{\mathrm{S1}}$, and R_2, $v^{\mathrm{St}}_{\mathrm{B2}}$ and $v^{\mathrm{St}}_{\mathrm{S2}}$ are also compared (Fig. 4). As wave propagation is from the north to south, this Stokes drift component is negative throughout the computational domain, with strongest values immediately outside the tidal inlet. For simulation R_1, the differences between $v^{\mathrm{St}}_{\mathrm{S1}}$ and $v^{\mathrm{St}}_{\mathrm{B1}}$ are small (Fig. 4c), while for R_2, northward Stokes drift estimates, $v^{\mathrm{St}}_{\mathrm{B2}}$ and $v^{\mathrm{St}}_{\mathrm{S2}}$ are at least twice of those from simulation R_1 (compare Figs. 4a and 4d, Figs. 4b and 4e). Theses differences are expected due to localized steepening and refraction of surface waves in the presence of opposing currents. The difference between $v^{\mathrm{St}}_{\mathrm{S2}}$ and $v^{\mathrm{St}}_{\mathrm{B2}}$ is also primarily localized to the tidal inlet region and may be up to 20% of the velocity magnitude (Fig. 4f).

4.3. Stokes Drift Profile and Wave Spectrum

For shallow water applications we have demonstrated that if only one-way coupling is considered (*i.e.,* simulation R_1), the Stokes drift estimates are similar for bulk or spectral formulation (Figs. 4c and Fig. 4d). Here, the role of two-way coupling in modifying Stokes drift estimates using spectral formulations (*i.e.,* $u^{\mathrm{St}}_{\mathrm{S1}}$, $u^{\mathrm{St}}_{\mathrm{S2}}$, $v^{\mathrm{St}}_{\mathrm{S1}}$ and $v^{\mathrm{St}}_{\mathrm{S2}}$) is considered, along with the vertical profile of Stokes drift, and the wave spectra $E(f, \theta)$. Particularly, the relative importance of two-way coupling in estimating Stokes drift is demonstrated by comparing near-surface eastward, $u^{\mathrm{St}}_{\mathrm{S2}}$ and northward, $v^{\mathrm{St}}_{\mathrm{S2}}$ Stokes drift for simulations R_1 and R_2 (Figs. 5a and 5b). The difference in the eastward Stokes drift ($u^{\mathrm{St}}_{\mathrm{S2}} - u^{\mathrm{St}}_{\mathrm{S1}}$) varies from 10^{-4}–10^{-3} ms^{-1} around the tidal inlet, while for the northward component of Stokes drift, $v^{\mathrm{St}}_{\mathrm{S2}} - v^{\mathrm{St}}_{\mathrm{S1}}$ the difference is of the order 10^{-3} ms^{-1}, *i.e.,* 10-20% of the Stokes drift magnitude.

We also expect differences in the vertical profile of eastward-directed ($u^{\mathrm{St}}_{\mathrm{B1}}(z), u^{\mathrm{St}}_{\mathrm{B2}}(z), u^{\mathrm{St}}_{\mathrm{S1}}(z)$ and $u^{\mathrm{St}}_{\mathrm{S2}}(z)$) and northward-directed ($v^{\mathrm{St}}_{\mathrm{B1}}(z), v^{\mathrm{St}}_{\mathrm{B2}}(z), v^{\mathrm{St}}_{\mathrm{S1}}(z)$ and $v^{\mathrm{St}}_{\mathrm{S2}}(z)$) Stokes-drift, considered at a location denoted by the green star in Fig. 5a. It is evident that for the simulations with one-way coupling, the eastward Stokes drift component estimates from bulk and spectral formulations have negligible vertical shear (Fig. 5c, solid green and dashed blue lines). For two-way coupled simulations the Stokes drift estimates of u^{St} changes sign and exhibits a strong near-surface shear (Fig. 5c, solid black and dashed red lines). The shear is stronger for the Stokes drift estimates using complete spectral formulations, $u^{\mathrm{St}}_{\mathrm{S2}}$ versus $u^{\mathrm{St}}_{\mathrm{B2}}$. The northward component of Stokes drift $v^{\mathrm{St}}_{\mathrm{B1}}$ and $v^{\mathrm{St}}_{\mathrm{S1}}$ have a similar vertical profile and shear (compare solid green and dashed blue lines, Fig. 5d). Near-surface $v^{\mathrm{St}}_{\mathrm{S2}}$ and $v^{\mathrm{St}}_{\mathrm{B2}}$ are at least 1.5× stronger than those estimated from one-way coupled simulations, with $v^{\mathrm{St}}_{\mathrm{S2}}$ exhibiting a stronger velocity shear (compare solid black and dashed red lines, Fig. 5d).

Current-induced wave refraction is expected to modify the surface wave spectra and the direction of wave propagation for simulation R_2, the ramifications of which are evident in $u^{\mathrm{St}}_{\mathrm{S2}} - u^{\mathrm{St}}_{\mathrm{S1}}$ and $v^{\mathrm{St}}_{\mathrm{S2}} - v^{\mathrm{St}}_{\mathrm{S1}}$, and the vertical profile of Stokes drift. The SWAN simulated wave spectra at the location corresponding to the vertical profiles of Stokes drift (*i.e.,* green square, Fig. 5a) is considered here. At lower frequencies (0.04-0.25 Hz), the $E(f)$ estimates from both one-way (green) and two-way (black) coupled simulations are similar (Fig. 5e). However, at higher frequencies, wave-current interactions modify $E(f)$. Even though this modification on $E(f)$ is small, Stokes drift estimates are heavily dependent on the high frequency components. Differences in wave propagation are also demonstrated by comparing the full frequency-directional spectra $E(f, \theta)$ for one-way (Fig. 5f) and two-way (Fig. 5e) coupled simulations. Refraction due to near-surface currents modifies the wave propagation direction as shown by change in energy content in the directional space.

Overall, simulations conducted for the shallow water tidal inlet demonstrate the importance of using both two-way coupling as well as the need to estimate Stokes drift using complete frequency-directional spectra.

5. Deep Water Idealized Hurricane Case

5.1. Significant Wave Height and Near-Surface Stokes drift

Hurricanes are associated with strong wind forcing, leading to generation of extreme waves in the ocean. Here, the wind forcing, U_{10} during the hurricane and associated significant wave height H_{s} are considered (Fig. 6). Within 100 km from the eye of the hurricane, wind speeds exceed 30 ms^{-1} (Fig. 6a). The significant wave height H_{s} reaches 14 m northeast of the hurricane center, and is relatively lower at the hurricane center and south of the hurricane. The magnitude of near-surface Stokes drift (*i.e.,* the topmost s layer) estimated using bulk formulations, $U_{\mathrm{B}}^{\mathrm{St}}$, deep-water approximations, $U_{\mathrm{Tran}}^{\mathrm{St}}$, $U_{\mathrm{Phil}}^{\mathrm{St}}$, and the spectral formulation, $U_{\mathrm{S}}^{\mathrm{St}}$ are compared (Fig. 7). Estimates from deep-water approximations ($U_{\mathrm{Tran}}^{\mathrm{St}}$ and $U_{\mathrm{Phil}}^{\mathrm{St}}$, Figs. 7b,c) have similar spatial patterns as those estimated using the complete directional spectrum $U_{\mathrm{S}}^{\mathrm{St}}$ (Fig. 7d). However, $U_{\mathrm{B}}^{\mathrm{St}}$ shows large deviation compared to $U_{\mathrm{S}}^{\mathrm{St}}$ (compare Figs. 7a and 7d).

Differences in the estimates of Stokes drift magnitude are further considered in Figs. 8a-8c. Although it is expected that the near-surface Stokes drift estimated using spectral formulations will be higher than those from the bulk formulation due to the contribution of the high frequency spectral region, yet we find that $U_{\mathrm{B}}^{\mathrm{St}}$ is greater than $U_{\mathrm{S}}^{\mathrm{St}}$ at the regions corresponding to higher waves, close to hurricane center (Fig. 8a). This occurs because $U_{\mathrm{B}}^{\mathrm{St}}$ ignores the directional wave spreading and the vertical decay is gradual in comparison to $U_{\mathrm{S}}^{\mathrm{St}}$ in the vertical direction [*e.g.,* see appendix, *Kumar et al.*, 2017]. The deviations ($U_{\mathrm{S}}^{\mathrm{St}}$- $U_{\mathrm{B}}^{\mathrm{St}}$) can reach up to 0.1ms^{-1}, *i.e.,* about 20% of the surface Stokes drift, which can cause a large error in estimating surface tracer trajectories and associated mixing processes, like Langmuir turbulence, by using the bulk formulation. Stokes drift estimates from $U_{\mathrm{Tran}}^{\mathrm{St}}$ are slightly greater than $U_{\mathrm{S}}^{\mathrm{St}}$, while those from $U_{\mathrm{Phil}}^{\mathrm{St}}$ are slightly smaller (compare figures Fig. 8b and 8c). The deviations between near-surface $U_{\mathrm{S}}^{\mathrm{St}}$ and the other three methods are shown as a probability density in Figs. 8d- 8f. The standard deviation between $U_{\mathrm{S}}^{\mathrm{St}}$ and $U_{\mathrm{B}}^{\mathrm{St}}$ is 0.027 ms^{-1} over the whole domain, which is almost twice the standard deviations for differences corresponding to $U_{\mathrm{Tran}}^{\mathrm{St}}$ and $U_{\mathrm{Phil}}^{\mathrm{St}}$.

In addition to differences in the magnitude of the Stokes drift, there are also implications for the Stokes drift direction. For example, the $U_{\mathrm{B}}^{\mathrm{St}}$ method, which is currently applied in the ROMS-SWAN coupled model, takes the mean wave direction in degrees as the Stokes drift direction, defined as

$$\theta_m = \arctan \frac{\int_0^{2\pi} \int_0^{\infty} \sigma N(\sigma,\theta) \sin\theta d\sigma d\theta}{\int_0^{2\pi} \int_0^{\infty} \sigma N(\sigma,\theta) \cos\theta d\sigma d\theta}. \tag{24}$$

The average deviation between the direction estimates for $U_{\mathrm{S}}^{\mathrm{St}}$ and $U_{\mathrm{B}}^{\mathrm{St}}$ reaches 26.85°, with a large standard deviation of 58.7° (Fig. 9a). This deviation is primarily due to the fact that the Stokes drift dependence on local winds is stronger at high frequencies than the low frequency wave component. By contrast, the $U_{\mathrm{Tran}}^{\mathrm{St}}$ and $U_{\mathrm{Phil}}^{\mathrm{St}}$ directions match well with the $U_{\mathrm{S}}^{\mathrm{St}}$ directions, with average deviation of -1.49°, and standard deviation of

48.7° (Figs. 9b,c). Overall, $U^{\mathrm{St}}_{\mathrm{Tran}}$ and $U^{\mathrm{St}}_{\mathrm{Phil}}$ methods perform much better than the $U^{\mathrm{St}}_{\mathrm{B}}$ method under hurricane forcing for both magnitude and direction of surface Stokes drift.

5.2. Stokes Drift Profiles

The implications of formulation choice (bulk, spectral, and super-exponential methods) on the estimates of the vertical profile of Stokes drift velocity magnitude U^{St} are considered for the different regions under hurricane forcing, *i.e.,* five locations with a distance of around 100 km from the hurricane center are chosen, as represented as red dots with the numbers (1 to 5), shown in Fig. 10a.

The vertical profile of Stokes drift magnitude ($U^{\mathrm{St}}_{\mathrm{B}}$, blue, $U^{\mathrm{St}}_{\mathrm{S}}$, black, $U^{\mathrm{St}}_{\mathrm{Phil}}$, green, and $U^{\mathrm{St}}_{\mathrm{Tran}}$, red) and the frequency-directional wave spectra corresponding to points 1 to 5 are shown in Figs. 10b-10f. Bulk estimates of U^{St} have weaker shear and a gradual vertical decay in comparison to $U^{\mathrm{St}}_{\mathrm{S}}$, $U^{\mathrm{St}}_{\mathrm{Phil}}$, and $U^{\mathrm{St}}_{\mathrm{Tran}}$ at all five locations (Figs. 10b-10f). In addition, the Stokes drift velocity magnitude $U^{\mathrm{St}}_{\mathrm{Phil}}$ has even stronger gradients than $U^{\mathrm{St}}_{\mathrm{S}}$ above 5 meters. This is because young seas of short fetch, and short duration hurricane storm forcing, have lower net contributions to near-surface shear from the wind sea spectrum than the fully developed seas approximated by $U^{\mathrm{St}}_{\mathrm{Phil}}$. Also, points 1 (Fig. 10b), 3 (Fig. 10d) and 5 (Fig. 10f) correspond to uni-modal wave spectra, and are dominated by the lower region of the frequency spectrum. For such cases, the values from $U^{\mathrm{St}}_{\mathrm{Phil}}$ are a better match with those of $U^{\mathrm{St}}_{\mathrm{S}}$ than $U^{\mathrm{St}}_{\mathrm{B}}$ and $U^{\mathrm{St}}_{\mathrm{Tran}}$ in the top 10 m of the water column. For cases with complex wave spectra, *e.g.,* with multi-directional and multimodal wave spectra (like Figs. 10c, 10e), the directional spreading and the high frequency part of the spectrum contribute significantly, affecting the Stokes drift profiles. Such cases typically correspond to strong Stokes drift shear in the upper ocean, *e.g.,* in the top 5 meters.

However, $U^{\mathrm{St}}_{\mathrm{B}}$ (blue lines) introduces substantial error in estimating the vertical Stokes shear and overestimates the surface Stokes drift because of the resulting slowly decaying vertical profiles. Moreover, we find that for such complex wave spectra, the $U^{\mathrm{St}}_{\mathrm{Phil}}$ and $U^{\mathrm{St}}_{\mathrm{Tran}}$ profiles provide good overall matches with that of $U^{\mathrm{St}}_{\mathrm{S}}$ for the whole water column. Considering that for $U^{\mathrm{St}}_{\mathrm{Phil}}$ and $U^{\mathrm{St}}_{\mathrm{Tran}}$, only the surface Stokes drift and Stokes transport are needed, it seems that they provide good approximations of the profiles resulting from the full wave spectrum Stokes drift, $U^{\mathrm{St}}_{\mathrm{S}}$.

The eastward and northward components of the Stokes drift at location 4 (Fig. 10) are considered as well (Fig. 11). The eastward component of Stokes drift is notably overestimated by $u^{\mathrm{St}}_{\mathrm{B}}$, while $u^{\mathrm{St}}_{\mathrm{Phil}}$ and $u^{\mathrm{St}}_{\mathrm{Tran}}$ estimated Stokes drift profiles agree well with that of $u^{\mathrm{St}}_{\mathrm{S}}$. For the v component of the Stokes drift profiles, the southward Stokes drift (negative values) are estimated by $v^{\mathrm{St}}_{\mathrm{Phil}}$ and $v^{\mathrm{St}}_{\mathrm{Tran}}$, which agree with that of $v^{\mathrm{St}}_{\mathrm{S}}$. However, $v^{\mathrm{St}}_{\mathrm{B}}$ is directed northward, which may induce errors in associated physical processes and dispersion of particles.

5.3. Vortex force

Vortex force plays an important role in the mean flow momentum balance [*Uchiyama et al.*, 2010b; *Kumar et al.*, 2012, 2013]. In a tropical cyclone, vortex force induced by the interaction between strong vorticity and the Stokes drift has the same order of magnitude as the horizontal advection. Furthermore, quasi-geostrophic circulation induced during and after the passage of the tropical cyclone is established and maintained by the vortex force [*Zhang et al.*, 2018].

Here, the vortex force is calculated for the four aforementioned simulations. The horizontal (J^{h}) and vertical(J^{v}) vortex force components for the simulation with Stokes drift estimated using spectral formulations (*i.e.,* $U_{\mathrm{S}}^{\mathrm{St}}$) are compared with the vortex force estimates ($J_{\mathrm{B}}^{\mathrm{h}}, J_{\mathrm{Tran}}^{\mathrm{h}}, J_{\mathrm{Phil}}^{\mathrm{h}}$) with Stokes drift calculated by the other three methods (*i.e.,* $U_{\mathrm{B}}^{\mathrm{St}}$, $U_{\mathrm{Tran}}^{\mathrm{St}}$ and $U_{\mathrm{Phil}}^{\mathrm{St}}$, Fig. 12). The horizontal vortex force estimated using the bulk formulation ($J_{\mathrm{B}}^{\mathrm{h}}$) is underestimated in comparison to the spectral estimates ($J_{\mathrm{S}}^{\mathrm{h}}$) at most of the locations within 100 km of the hurricane center (Fig. 12a). Differences between $J_{\mathrm{S}}^{\mathrm{h}}$ and $J_{\mathrm{B}}^{\mathrm{h}}$ are of the order $\mathcal{O}(10^{-5})$. The difference between $J_{\mathrm{S}}^{\mathrm{h}}$ and the horizontal vortex force estimated using the super-exponential approaches (*i.e.,* $J_{\mathrm{Tran}}^{\mathrm{h}}$ and $J_{\mathrm{Phil}}^{\mathrm{h}}$) are also considered (Figs. 12b, c) and in general have similar spatial patterns, with underestimation immediately south, and overestimation east and west of the hurricane center. However, in comparison to the estimates using bulk formulations, these differences are of lower order, *i.e.,* $\mathcal{O}(10^{-6})$.

The vertical component of the vortex force, J^{v} may also play a role in the momentum balance (*e.g.,* see Eqs. 2, 3). Here, the vertical component of the vortex force from the spectral estimates, $J_{\mathrm{S}}^{\mathrm{v}}$ are compared to the bulk, $J_{\mathrm{B}}^{\mathrm{v}}$ and the super-exponential approach, $J_{\mathrm{Tran}}^{\mathrm{v}}$ and $J_{\mathrm{Phil}}^{\mathrm{v}}$ (Figs. 12d-12f). The bulk approach overestimates J^{v} at most locations around the hurricane center, while $J_{\mathrm{Tran}}^{\mathrm{v}}$ and $J_{\mathrm{Phil}}^{\mathrm{v}}$ are slightly smaller than $J_{\mathrm{S}}^{\mathrm{v}}$ east of the hurricane center, and relatively larger to the south and north. Furthermore, $J_{\mathrm{S}}^{\mathrm{v}} - J_{\mathrm{Phil}}^{\mathrm{v}}, J_{\mathrm{S}}^{\mathrm{v}} - J_{\mathrm{Tran}}^{\mathrm{v}}$ are of the order $\mathcal{O}(10^{-7})$, *i.e.,* an order smaller than $J_{\mathrm{S}}^{\mathrm{v}} - J_{\mathrm{B}}^{\mathrm{v}}$ (Figs. 12d-f). These results suggest that models using super-exponential Stokes drift methods can perform much better than those using monochromatic bulk estimates under hurricane forcing in deep waters.

In order to further determine the importance of the Stokes drift based terms in the momentum balance, the zonal ($J_{1\mathrm{S}}^{\mathrm{h}}, J_{1\mathrm{S}}^{\mathrm{v}}$) and meridional ($J_{2\mathrm{S}}^{\mathrm{h}}, J_{2\mathrm{S}}^{\mathrm{v}}$) vortex force estimates from the spectral formulations are compared to the local and advective acceleration, as shown in Fig. 13. Particularly, both horizontal and vertical vortex force components in longitudinal and meridional directions (Fig. 13a-13d) are of the order $\mathcal{O}(10^{-5}-10^{-7})\mathrm{ms}^{-2}$ and similar to or larger than the local and advective acceleration terms (Fig. 13e-13h). Considering that the Stokes drift can be of the order, $\mathcal{O}(10^{-1}\mathrm{ms}^{-1})$, these terms which are dependent on the Stokes drift are important and contribute to the momentum balance.

6. Summary and conclusion

Stokes drift plays essential roles in the upper ocean mixing and dispersion that require accurate representation of its vertical profile. This study implements and tests a method to compute Stokes drift by discrete integration over the frequency-directional surface wave spectra in the context of coupled wave-ocean simulations using SWAN and ROMS in the COAWST framework. This more complete spectral representation is compared to the prior monochromatic approximation by a single exponential function matching bulk wave parameters, as well as to two super-exponential functions proposed by *Breivik et al.* [2014, 2016] to estimate the Stokes drift profile for fully developed wind seas. The impact of these four approaches on estimating Stokes drift is examined in the context of both one-way and two-way wave-ocean coupling, and in the context of two different and long-standing COAWST modeling test cases: One shallow-water case without wind forcing where offshore swell refracts and interacts with the bathymetry and with the tidally driven current in a coastal inlet, and one deep-water case where the strong transient wind forcing of a passing hurricane produces young wind seas that deviate from the spectra of fully developed equilibrium wind seas of unidirectional steady forcing.

For the shallow inlet test case, interactions with currents significantly modify the wave spectrum in two-way coupled simulations, relative to just one-way coupling from waves to currents. It is therefore necessary to fully couple waves to the ocean model when estimating the Stokes drift, even in this case without wind forcing. Simulations for the shallow water inlet test case show that the Stokes drift from the full spectrum formulation, u^{St}_{Spec} provides Stokes drift profiles with strong gradients, while that resulting from the bulk formulation, u^{St}_{Bulk} cannot provide such rapidly decaying Stokes drift profiles, as it neglects contributions from the high frequency part of the directional wave spectrum. It is strongly recommended that the Stokes drift profiles calculated as u^{St}_{Spec} from the full wave spectra should be applied in wave-current studies for nearshore regions. The need to calculate Stokes drift as u^{St}_{Spec} rather than u^{St}_{Bulk} can only be expected to increase where wind forcing is also applied in shallow-water nearshore areas.

For the deep water, idealized hurricane test case, the monochromatic bulk approximation u^{St}_{Bulk} significantly underestimates the vertical gradient of Stokes drift, and also leads to significant error in the Stokes drift direction. Our overall recommendation is that the u^{St}_{Spec} spectral method is still generally the most accurate method for deep water studies of transient wind-driven events, like wave-current interactions under hurricanes or storms. This method ensures more accurate estimates of Stokes drift-associated dynamical processes, *e.g.,* vortex force and Stokes-Coriolis force. The u^{St}_{Tran} and u^{St}_{Phil} super-exponential approximations agree relatively well with u^{St}_{Spec}, even with hurricane-generated complicated wave spectrum. However this approach appears best-suited for long time-scale runs, relative to wave growth rates, and perhaps for simulations with low temporal resolution of wind forcing. These super-exponential approximations u^{St}_{Tran} and u^{St}_{Phil} perform much better than u^{St}_{Bulk}, and only require two bulk parameters from the wave model, generally much less than is required for u^{St}_{Spec}. On the other hand, the additional computational overhead of u^{St}_{Spec} appears minor in our test cases.

In previous versions of the COAWST system, only the u^{St}_{Bulk} method has been available. This approximation limits the prospects for wave-current interaction studies and the exploration of more precise roles of vortex force and Coriolis-Stokes effects in the upper ocean dynamics. The newly implemented methods for estimating Stokes drift in the ROMS-SWAN coupled model provide unique opportunities to develop better understanding of these Stokes drift associated dynamical processes in ocean dynamics, tracer Lagrangian trajectories and related studies. Thus, it also becomes possible to properly introduce ocean mixing parameterizations of processes driven by Stokes drift forcing, such as Langmuir turbulence, into the the ROMS ocean model.

Appendix A: The computational cost of transferring and estimating the Stokes drift profiles

By using the same computational environment, Intel Xeon E3-1535M v5 @2.9 GHz, as an example, we run the Inlet test 2-way case, with four different methods of estimating the Stokes drift profile. All the computational costs are listed in Table 2. It is found that $u^{\mathrm{St}}_{\mathrm{Tran}}$ and $u^{\mathrm{St}}_{\mathrm{Phil}}$ methods cost the same time, just 11 seconds, or 2.5% longer than the 7 min 14 sec required for the $u^{\mathrm{St}}_{\mathrm{B}}$ method. That is because 4 more parameters (x, y-components of surface Stokes drift and Stokes transport) are transferred from SWAN to ROMS than the bulk approach. For the spectral method to estimate $u^{\mathrm{St}}_{\mathrm{S}}$ method, it costs 7 min 30 seconds, or 3.7% longer than $u^{\mathrm{St}}_{\mathrm{B}}$, because more data including Stokes drift spectrum, and wave numbers are transferred to ROMS. Note, the data transfer requirement increases with the number of frequency bins used in SWAN, and with the the computational grid cells.

Acknowledgments. We thank John Warner from United States Geological Survey Coastal and Marine Science Center for useful suggestions. All the data are generated by the open-source COAWST modeling system. The configurations and parameters used for all the runs are detailed described in Section 3. G. Liu was supported, in part the National Key Research and Development Program of China 2016YFC1401407; National Natural Science Foundation of China under Grant 41506028; Natural Science Foundation of Jiangsu Province under Grant BK20150913; the Startup Foundation for Introducing Talent of NUIST; the International cooperation project of National Natural Science Foundation of China under Grant 41620104003; National Program on Global Change and Air-Sea Interaction under Grant GASI-IPOVAI-04; R. Harcourt was supported, in part, by NSF OCE-1558459 and OCE-1756115, and a by grant from the Gulf of Mexico Research Initiative (SA-15-15). W. Perrie was supportted by the Office of Energy Research and Development (OERD) project 1B00.003C; the Canadian Space Agency Data Utilization and Applications Program (DUAP) project 14SURM006; the SWOT program, MEOPAR (Marine Environmental Observation Prediction and Response Network) project 1P1.2 and in part by National Natural Science Youth Foundation of China under Grant 41706193.

References

Akan, Ç., S. Moghimi, H. T. Özkan-Haller, J. Osborne, and A. Kurapov (2017), On the dynamics of the mouth of the Columbia River: Results from a three-dimensional fully coupled wave-current interaction model, *Journal of Geophysical Research: Oceans*, *122*(7), 5218–5236.

Ardhuin, F., N. Rascle, and K. A. Belibassakis (2008), Explicit wave-averaged primitive equations using a generalized lagrangian mean, *Ocean Modelling*, *20*(1), 35–60.

Ardhuin, F., L. Marié, N. Rascle, P. Forget, and A. Roland (2009), Observation and estimation of lagrangian, stokes, and eulerian currents induced by wind and waves at the sea surface, *Journal of Physical Oceanography*, *39*(11), 2820–2838.

Bennis, A.-C., F. Ardhuin, and F. Dumas (2011), On the coupling of wave and three-dimensional circulation models: Choice of theoretical framework, practical implementation and adiabatic tests, *Ocean Modelling*, *40*(3-4), 260–272.

Black, P. G., E. A. D'Asaro, W. M. Drennan, J. R. French, P. P. Niiler, T. B. Sanford, E. J. Terrill, E. J. Walsh, and J. A. Zhang (2007), Air–sea exchange in hurricanes: Synthesis of observations from the coupled boundary layer air–sea transfer experiment, *Bulletin of the American Meteorological Society*, *88*(3), 357–374.

Booij, N., R. Ris, and L. H. Holthuijsen (1999), A third-generation wave model for coastal regions: 1. Model description and validation, *Journal of geophysical research: Oceans*, *104*(C4), 7649–7666.

Booij, N., I. Haagsma, L. a. Holthuijsen, A. Kieftenburg, R. Ris, A. vd Westhuysen, and M. Zijlema (2004), Swan user manual, swan cycle iii version 40.41, *Delft University of Technology*.

Breivik, O., A. A. Allen, C. Maisondieu, J.-C. Roth, and B. Forest (2012), The leeway of shipping containers at different immersion levels, *Ocean Dynamics*, *62*(5), 741–752.

Breivik, Ø., P. A. Janssen, and J.-R. Bidlot (2014), Approximate stokes drift profiles in deep water, *Journal of Physical Oceanography*, *44*(9), 2433–2445.

Breivik, Ø., J.-R. Bidlot, and P. A. Janssen (2016), A Stokes drift approximation based on the phillips spectrum, *Ocean Modelling*, *100*, 49–56.

Craik, A. D., and S. Leibovich (1976), A rational model for langmuir circulations, *Journal of Fluid Mechanics*, *73*(3), 401–426.

Crosby, S. C., N. Kumar, W. OReilly, and R. Guza (2019), Regional swell transformation by backward ray tracing and swan, *Journal of Atmospheric and Oceanic Technology*, *36*(2), 217–229.

Curcic, M., S. S. Chen, and T. M. Özgökmen (2016), Hurricane-induced ocean waves and Stokes drift and their impacts on surface transport and dispersion in the Gulf of Mexico, *Geophysical Research Letters*, *43*(6), 2773–2781.

D'Asaro, E. A., J. Thomson, A. Y. Shcherbina, R. R. Harcourt, M. F. Cronin, M. A. Hemer, and B. Fox-Kemper (2014), Quantifying upper ocean turbulence driven by surface waves, *Geophysical Research Letters*, *41*(1), 102–107.

Deike, L., N. Pizzo, and W. K. Melville (2017), Lagrangian transport by breaking surface waves, *Journal of Fluid Mechanics*, *829*, 364–391.

Fan, Y., I. Ginis, T. Hara, C. W. Wright, and E. J. Walsh (2009), Numerical simulations and observations of surface wave fields under an extreme tropical cyclone, *Journal of Physical Oceanography*, *39*(9), 2097–2116.

Faria, A. F., E. B. Thornton, T. C. Lippmann, and T. P. Stanton (2000), Undertow over a barred beach, *Journal of Geophysical Research: Oceans*, *105*(C7), 16,999–17,010.

Gradshteyn, I. S., and I. M. Ryzhik (2007), Table of Integrals, Series, and Products. Edited by A. Jeffrey and D. Zwillinger.

Harcourt, R. R. (2013), A second-moment closure model of Langmuir turbulence, *Journal of Physical Oceanography*, *43*(4), 673–697.

Harcourt, R. R. (2015), An improved second-moment closure model of Langmuir turbulence, *Journal of Physical Oceanography*, *45*(1), 84–103.

Harcourt, R. R., and E. A. D'Asaro (2008), Large-eddy simulation of Langmuir turbulence in pure wind seas, *Journal of Physical Oceanography*, *38*(7), 1542–1562.

Hasselmann, K. (1970), Wave-driven inertial oscillations, *Geophysical and Astrophysical Fluid Dynamics*, *1*(3-4), 463–502.

Holland, G. J. (1980), An analytic model of the wind and pressure profiles in hurricanes, *Monthly weather review*, *108*(8), 1212–1218.

Janssen, P. (2004), *The interaction of ocean waves and wind*, Cambridge University Press.

Kenyon, K. E. (1969), Stokes drift for random gravity waves, *Journal of Geophysical Research*, *74*(28), 6991–6994.

Kirby, J. T., and T.-M. Chen (1989), Surface waves on vertically sheared flows: approximate dispersion relations, *Journal of Geophysical Research: Oceans*, *94*(C1), 1013–1027.

Kumar, N., and F. Feddersen (2017), The effect of Stokes drift and transient rip currents on the inner shelf. part i: No stratification, *Journal of Physical Oceanography*, *47*(1), 227–241.

Kumar, N., G. Voulgaris, J. C. Warner, and M. Olabarrieta (2012), Implementation of the vortex force formalism in the coupled ocean-atmosphere-wave-sediment transport (COAWST) modeling system for inner shelf and surf zone applications, *Ocean Modelling*, *47*, 65–95.

Kumar, N., G. Voulgaris, J. H. List, and J. C. Warner (2013), Alongshore momentum balance analysis on a cuspate foreland, *Journal of Geophysical Research: Oceans*, *118*(10), 5280–5295.

Kumar, N., F. Feddersen, Y. Uchiyama, J. McWilliams, and W. OReilly (2015), Midshelf to surfzone coupled roms–swan model data comparison of waves, currents, and temperature: Diagnosis of subtidal forcings and response, *Journal of Physical Oceanography*, *45*(6), 1464–1490.

Kumar, N., D. L. Cahl, S. C. Crosby, and G. Voulgaris (2017), Bulk versus spectral wave parameters: Implications on stokes drift estimates, regional wave modeling, and hf radars applications, *Journal of Physical Oceanography*, *47*(6), 1413–1431.

Lentz, S. J., M. Fewings, P. Howd, J. Fredericks, and K. Hathaway (2008), Observations and a model of undertow over the inner continental shelf, *Journal of Physical Oceanography*, *38*(11), 2341–2357.

Levitus, S., R. A. Locarnini, T. P. Boyer, A. V. Mishonov, J. I. Antonov, H. E. Garcia, O. K. Baranova, M. M. Zweng, D. R. Johnson, and D. Seidov (2002), World ocean atlas 2009.

Li, Q., and B. Fox-Kemper (2017), Assessing the effects of langmuir turbulence on the entrainment buoyancy flux in the ocean surface boundary layer, *Journal of Physical Oceanography*, *47*(12), 2863–2886.

Liu, G., W. A. Perrie, and Y. He (2014), Ocean surface Stokes drift from scatterometer observations, *International journal of remote sensing*, *35*(5), 1966–1978.

Longuet-Higgins, M. S., D. Cartwright, and N. Smit (1963), Observations of the directional spectrum of sea waves using the motions of a floating buoy, *Ocean Wave Spectra:*

Proceedings of a Conference.

Marchesiello, P., R. Benshila, R. Almar, Y. Uchiyama, J. C. McWilliams, and A. Shchepetkin (2015), On tridimensional rip current modeling, *Ocean Modelling*, *96*, 36–48.

McWilliams, J. C. (2018), Surface wave effects on submesoscale fronts and filaments, *Journal of Fluid Mechanics*, *843*, 479–517.

McWilliams, J. C., and B. Fox-Kemper (2013), Oceanic wave-balanced surface fronts and filaments, *Journal of Fluid Mechanics*, *730*, 464–490.

McWilliams, J. C., and J. M. Restrepo (1999), The wave-driven ocean circulation, *Journal of Physical Oceanography*, *29*(10), 2523–2540.

McWilliams, J. C., and P. P. Sullivan (2000), Vertical mixing by langmuir circulations, *Spill Science & Technology Bulletin*, *6*(3-4), 225–237.

McWilliams, J. C., P. P. Sullivan, and C.-H. Moeng (1997), Langmuir turbulence in the ocean, *Journal of Fluid Mechanics*, *334*, 1–30.

McWilliams, J. C., J. M. Restrepo, and E. M. Lane (2004), An asymptotic theory for the interaction of waves and currents in coastal waters, *Journal of Fluid Mechanics*, *511*, 135–178.

Moghimi, S., K. Klingbeil, U. Gräwe, and H. Burchard (2013), A direct comparison of a depth-dependent radiation stress formulation and a vortex force formulation within a three-dimensional coastal ocean model, *Ocean Modelling*, *70*, 132–144.

Moghimi, S., H. T. Özkan-Haller, Ç. Akan, and J. T. Jurisa (2019), Mechanistic analysis of the wave-current interaction in the plume region of a partially mixed tidal inlet, *Ocean Modelling*, *134*, 110–126.

Olabarrieta, M., J. C. Warner, and N. Kumar (2011), Wave-current interaction in Willapa Bay, *Journal of Geophysical Research: Oceans*, *116*(C12).

Olabarrieta, M., J. C. Warner, B. Armstrong, J. B. Zambon, and R. He (2012), Ocean–atmosphere dynamics during Hurricane Ida and Nor'Ida: an application of the coupled ocean–atmosphere–wave–sediment transport (COAWST) modeling system, *Ocean Modelling*, *43*, 112–137.

Phillips, O. (1985), Spectral and statistical properties of the equilibrium range in wind-generated gravity waves, *Journal of Fluid Mechanics*, *156*, 505–531.

Phillips, O. M. (1958), The equilibrium range in the spectrum of wind-generated waves, *Journal of Fluid Mechanics*, *4*(4), 426–434.

Phillips, O. M. (1966), *The dynamics of the upper ocean*, CUP Archive.

Polton, J. A., D. M. Lewis, and S. E. Belcher (2005), The role of wave-induced Coriolis-Stokes forcing on the wind-driven mixed layer, *Journal of Physical Oceanography*, *35*(4), 444–457.

Rascle, N., F. Ardhuin, P. Queffeulou, and D. Croizé-Fillon (2008), A global wave parameter database for geophysical applications. part 1: Wave-current-turbulence interaction parameters for the open ocean based on traditional parameterizations, *Ocean Modelling*, *25*(3-4), 154–171.

Reichl, B. G., D. Wang, T. Hara, I. Ginis, and T. Kukulka (2016a), Langmuir turbulence parameterization in tropical cyclone conditions, *Journal of Physical Oceanography*, *46*(3), 863–886.

Reichl, B. G., I. Ginis, T. Hara, B. Thomas, T. Kukulka, and D. Wang (2016b), Impact of sea-state-dependent Langmuir turbulence on the ocean response to a tropical cyclone, *Monthly Weather Review*, *144*(12), 4569–4590.

Röhrs, J., K. H. Christensen, L. R. Hole, G. Broström, M. Drivdal, and S. Sundby (2012), Observation-based evaluation of surface wave effects on currents and trajectory forecasts, *Ocean Dynamics*, *62*(10-12), 1519–1533.

Röhrs, J., A. K. Sperrevik, K. H. Christensen, G. Broström, and O. Breivik (2015), Comparison of hf radar measurements with eulerian and lagrangian surface currents, *Ocean Dynamics*, *65*(5), 679–690.

Saetra, Ø., J. Albretsen, and P. A. Janssen (2007), Sea-state-dependent momentum fluxes for ocean modeling, *Journal of Physical Oceanography*, *37*(11), 2714–2725.

Shchepetkin, A. F., and J. C. McWilliams (2005), The regional oceanic modeling system (ROMS): a split-explicit, free-surface, topography-following-coordinate oceanic model, *Ocean modelling*, *9*(4), 347–404.

Stokes, S. G. G. (1847), *Supplement to a memoir on some cases of fluid motion*, Printed at the Pitt Press by John W. Parker.

Sullivan, P. P., and J. C. McWilliams (2010), Dynamics of winds and currents coupled to surface waves, *Annual Review of Fluid Mechanics*, *42*.

Suzuki, N., B. Fox-Kemper, P. E. Hamlington, and L. P. Van Roekel (2016), Surface waves affect frontogenesis, *Journal of Geophysical Research: Oceans*, *121*(5), 3597–3624.

Tamura, H., Y. Miyazawa, and L.-Y. Oey (2012), The Stokes drift and wave induced-mass flux in the north pacific, *Journal of Geophysical Research: Oceans*, *117*(C8).

Thorpe, S. A. (2004), Langmuir circulation, *Annu. Rev. Fluid Mech.*, *36*, 55–79.

Uchiyama, Y., J. C. McWilliams, and A. F. Shchepetkin (2010a), Wave-current interaction in an oceanic circulation model with a vortex-force formalism: Application to the surf zone, *Ocean Modelling*, *34* (1-2), 16–35.

Uchiyama, Y., J. C. McWilliams, and A. F. Shchepetkin (2010b), Wave-current interaction in an oceanic circulation model with a vortex-force formalism: Application to the surf zone, *Ocean Modelling*, *34* (1-2), 16–35.

Umlauf, L., and H. Burchard (2003), A generic length-scale equation for geophysical turbulence models, *Journal of Marine Research*, *61* (2), 235–265.

Ursell, F., and G. Deacon (1950), On the theoretical form of ocean swell. on a rotating earth, *Geophysical Journal International*, *6*, 1–8.

van den Bremer, T. S., and . O. Breivik (2018), Stokes drift, *Phil. Trans. R. Soc. A*, *376* (2111), 20170,104.

Warner, J. C., C. R. Sherwood, H. G. Arango, and R. P. Signell (2005), Performance of four turbulence closure models implemented using a generic length scale method, *Ocean Modelling*, *8* (1-2), 81–113.

Warner, J. C., C. R. Sherwood, R. P. Signell, C. K. Harris, and H. G. Arango (2008), Development of a three-dimensional, regional, coupled wave, current, and sediment-transport model, *Computers & Geosciences*, *34* (10), 1284–1306.

Warner, J. C., B. Armstrong, R. He, and J. B. Zambon (2010), Development of a coupled ocean-atmosphere-wave-sediment transport (COAWST) modeling system, *Ocean modelling*, *35* (3), 230–244.

Webb, A., and B. Fox-Kemper (2011), Wave spectral moments and stokes drift estimation, *Ocean modelling*, *40* (3-4), 273–288.

Webb, A., and B. Fox-Kemper (2015), Impacts of wave spreading and multidirectional waves on estimating Stokes drift, *Ocean Modelling*, *96*, 49–64.

Wu, L., A. Rutgersson, and E. Sahlée (2015), Upper-ocean mixing due to surface gravity waves, *Journal of Geophysical Research: Oceans*, *120*(12), 8210–8228.

Zambon, J. B., R. He, and J. C. Warner (2014), Investigation of hurricane Ivan using the coupled ocean–atmosphere–wave–sediment transport (COAWST) model, *Ocean Dynamics*, *64*(11), 1535–1554.

Zhang, X., P. Chu, W. Li, C. Liu, L. Zhang, C. Shao, X. Zhang, G. Chao, and Y. Zhao (2018), Impact of Langmuir turbulence on the thermal response of the ocean mixed layer to super typhoon haitang (2005), *Journal of Physical Oceanography*.

Zijlema, M., G. P. Van Vledder, and L. Holthuijsen (2012), Bottom friction and wind drag for wave models, *Coastal Engineering*, *65*, 19–26.

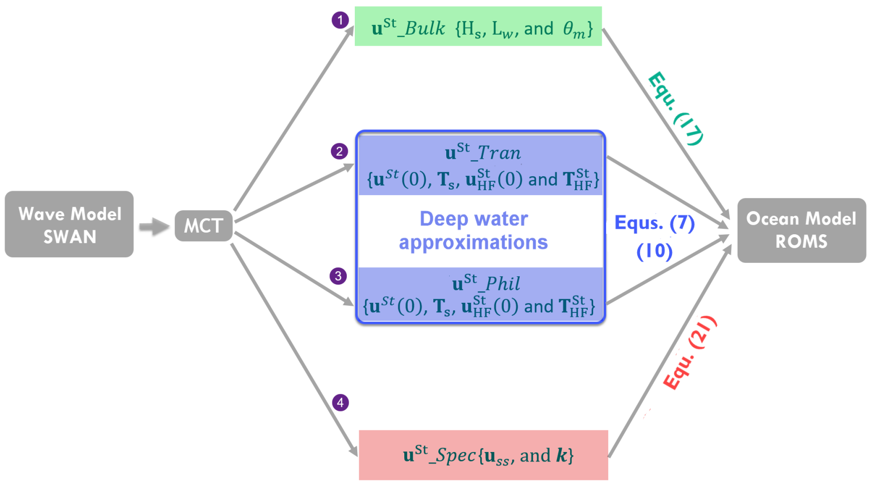

Figure 1. Schematic illustration of four methods of estimating Stokes drift profiles for coupled ROMS-SWAN model

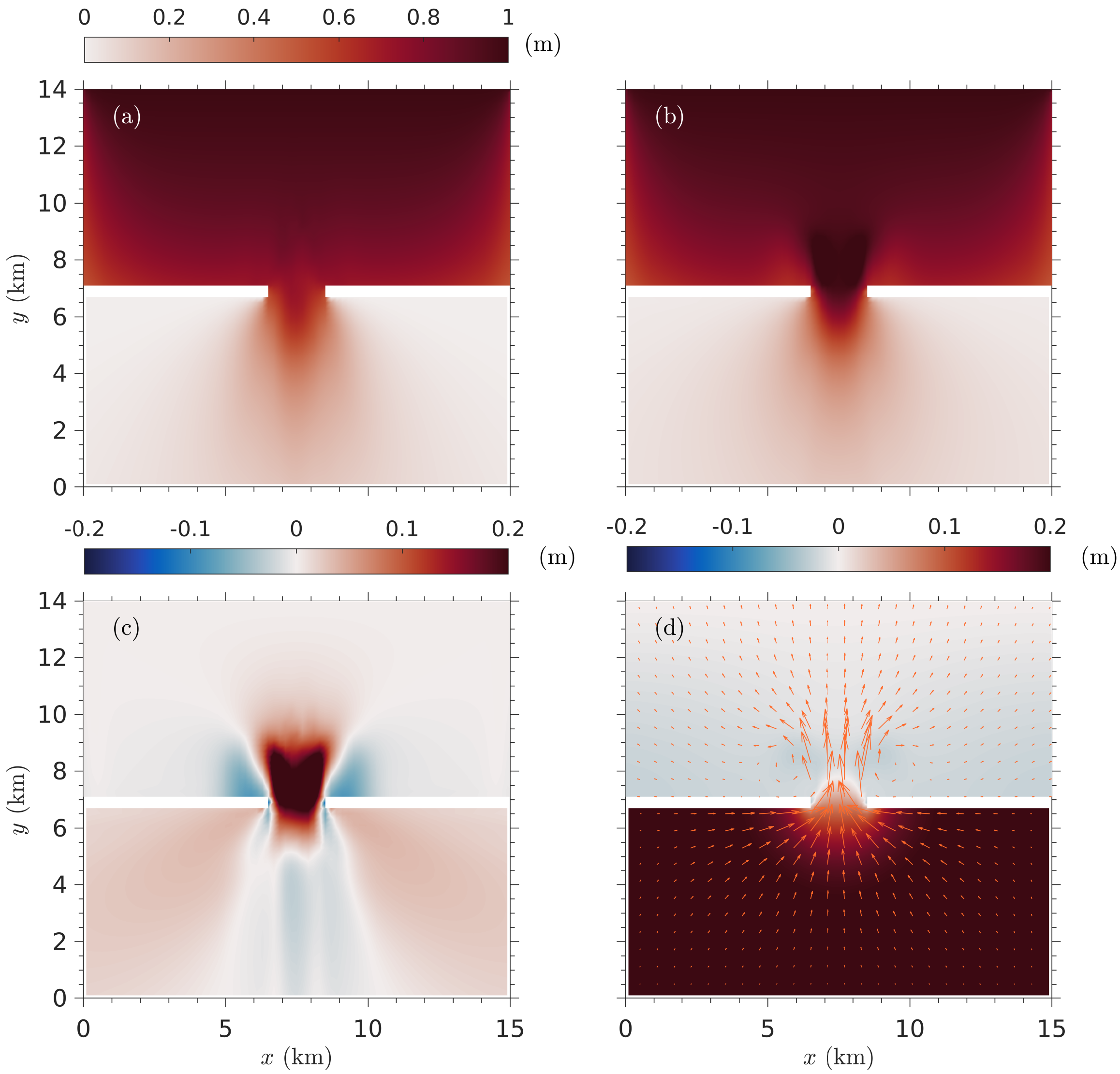

Figure 2. Significant wave height H_s (color shading) versus cross-shore (x) and along-shore (y) coordinates for (a) one-way (R_1); and (b) two-way (R_2) coupled simulations. (c) color shading showing the difference in H_s (*i.e.*, $H_s|_{R_2} - H_s|_{R_1}$); and (d) mean sea-surface elevation (η, color shading) with tidal currents (orange arrows) overlaid. All results are shown after a simulation period of 12 hours. The offshore boundary is located at $y = 14$ km, and the white spaces in (a-d) are masked. The back-barrier region from $y = 0 - 6.5$km has a constant depth of 4 m.

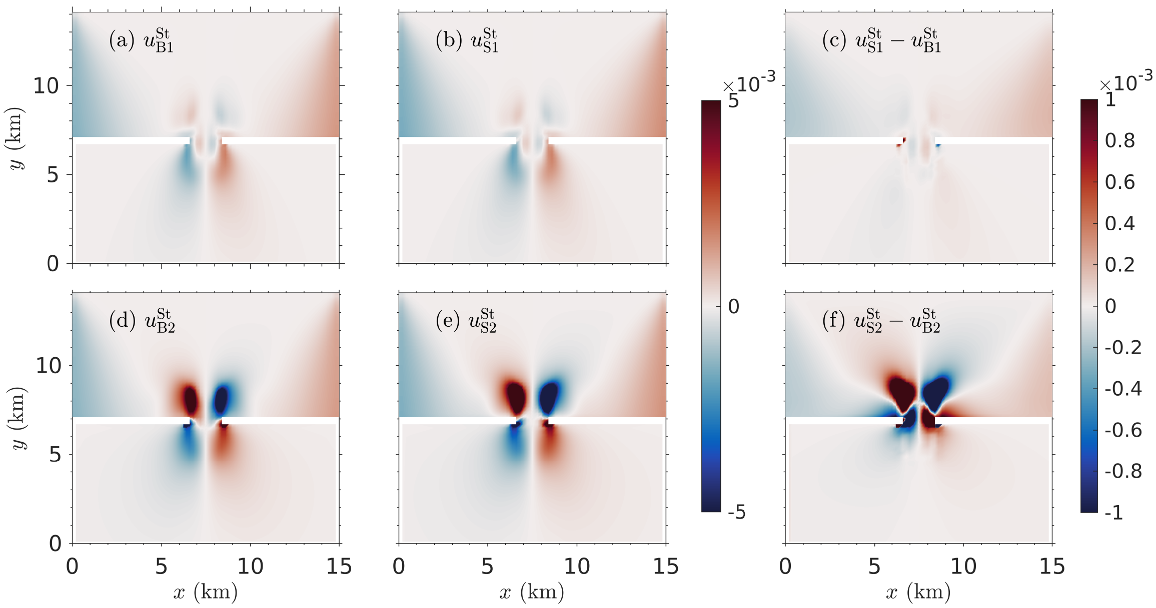

Figure 3. Cross-shore component of near-surface Stokes drift (color shading) versus cross-shore (x) and alongshore (y) coordinates for one-way (a-b, R_1) and two-way coupled (d-e, R_2) simulations. Stokes drift estimates in (a) and (d) are from bulk formulations (Eq. 17), while those in (b) and (e) are from spectral formulation (Eq. 21). Color shading indicating the differences between spectral and bulk estimate of near-surface Stokes drift for one-way (*i.e.*, $u^{\mathrm{St}}_{\mathrm{S1}} - u^{\mathrm{St}}_{\mathrm{B1}}$) and two-way (*i.e.*, $u^{\mathrm{St}}_{\mathrm{S2}} - u^{\mathrm{St}}_{\mathrm{B2}}$) coupled simulations are shown in (c) and (f), respectively. Note that the near-surface Stokes drift is from the ROMS s layer closest to the mean sea-surface. Also, note that the colorbar for (a, b, d and e) are different than (c, f).

v_stokes_inlet_test.pdf

Figure 4. Same as Fig. 3, but for alongshore component of Stokes drift.

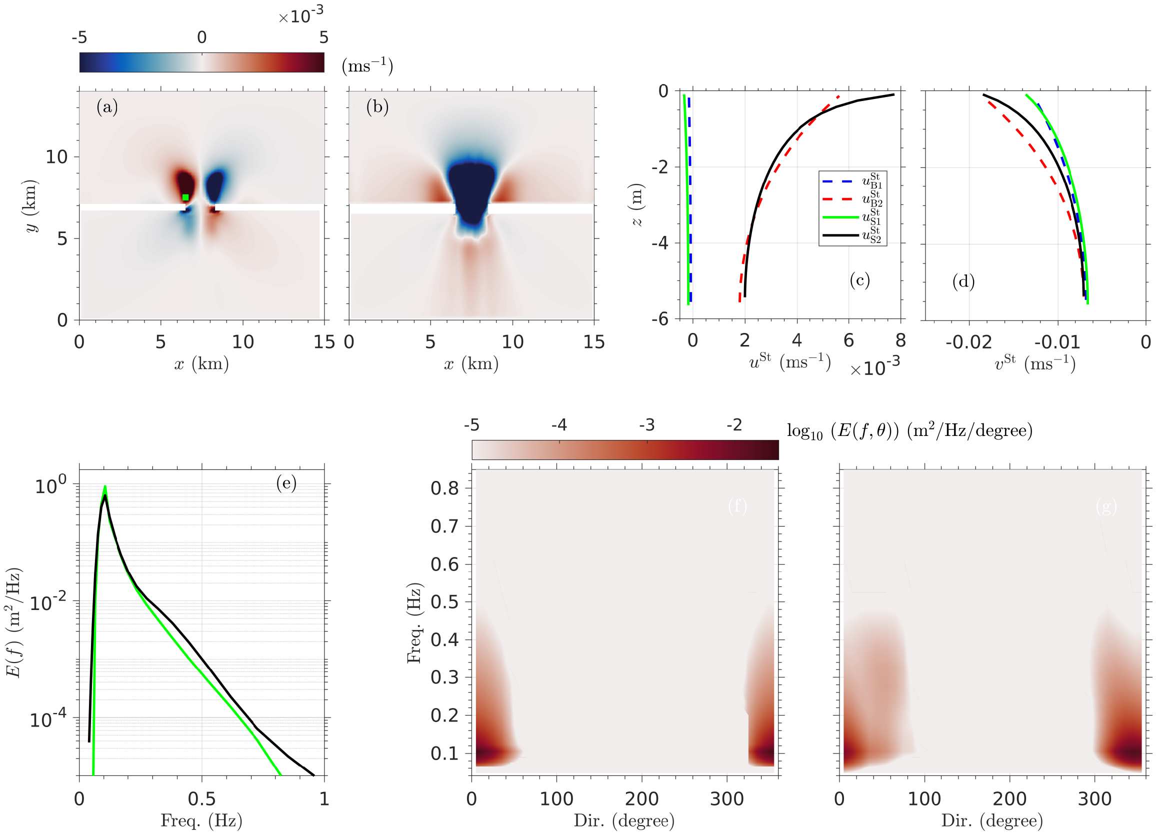

Figure 5. Color shading indicating the difference between two-way and one-way coupled model simulation based estimates of near-surface (a) cross-shore, and (b) alongshore Stokes drift estimated using spectral formulations, *i.e.*, $u^{\rm St}_{\rm S2} - u^{\rm St}_{\rm S1}$ and $v^{\rm St}_{\rm S2} - v^{\rm St}_{\rm S1}$. Vertical profile of (c) cross-shore and (d) alongshore Stokes drift, and (e) wave energy versus frequency at the location indicated by green square in (a). In (c) and (d) solid lines represent spectral estimates, while dashed lines are bulk estimates. Also dashed blue and green correspond to one-way coupled, while dashed red and black correspond to two-way coupled simulations. The complete frequency-directional spectra are also shown for one-way (f) and two-way (g) coupled simulations.

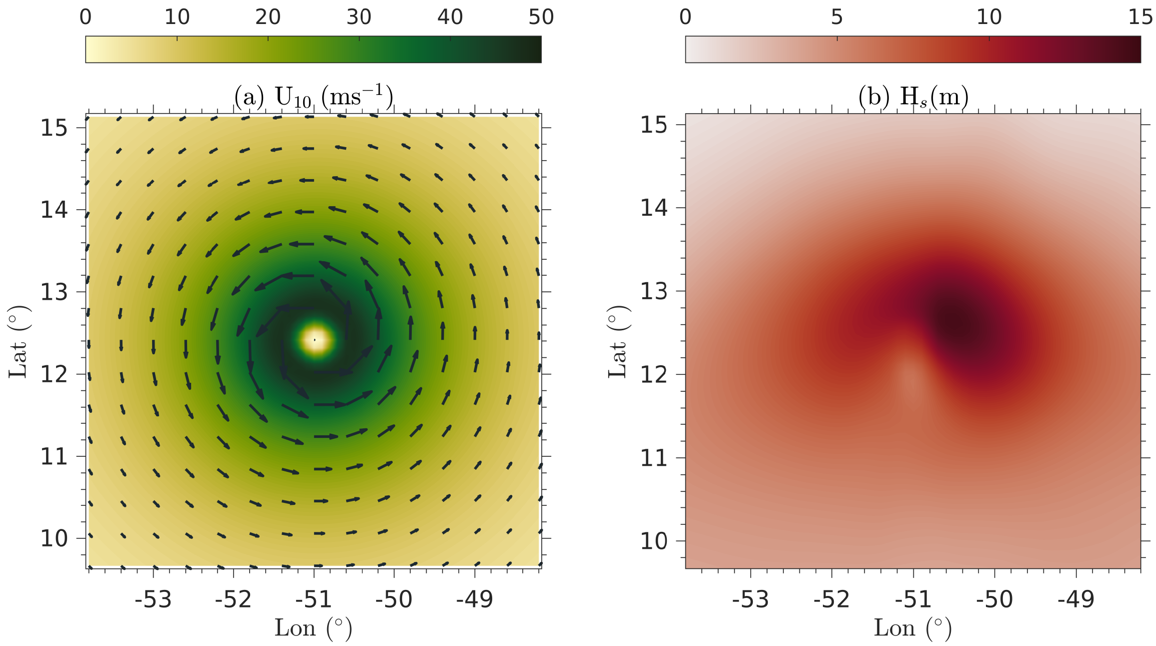

Figure 6. (a) Hurricane wind forcing U_{10} and (b) Significant wave height H_s.

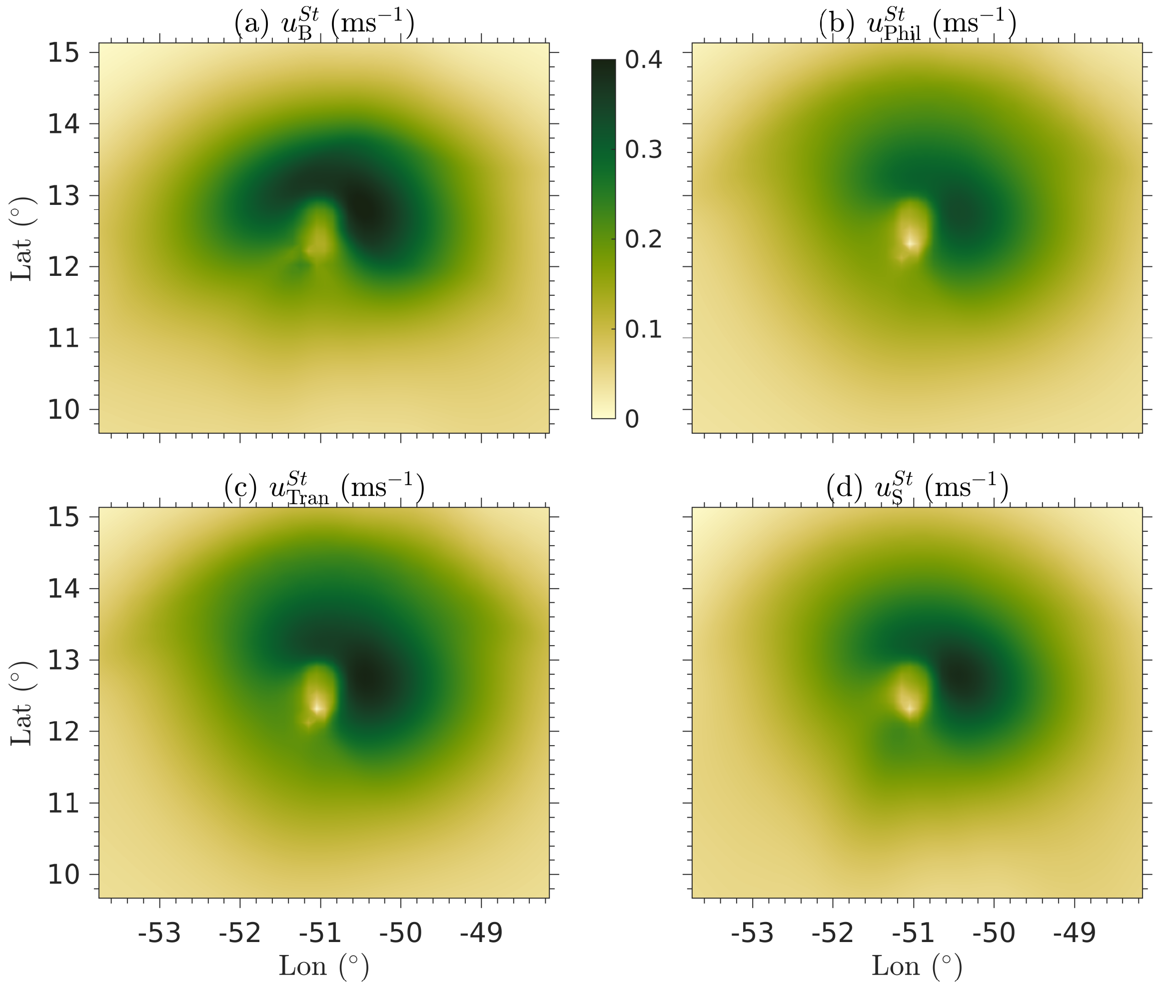

Figure 7. Near-surface Stokes drift magnitude (color shading) (a) $U_{\mathrm{B}}^{\mathrm{St}}$; (b) $U_{\mathrm{Phil}}^{\mathrm{St}}$; (c) $U_{\mathrm{Tran}}^{\mathrm{St}}$; and (d) $U_{\mathrm{S}}^{\mathrm{St}}$ versus longitude and latitude for the idealized hurricane case.

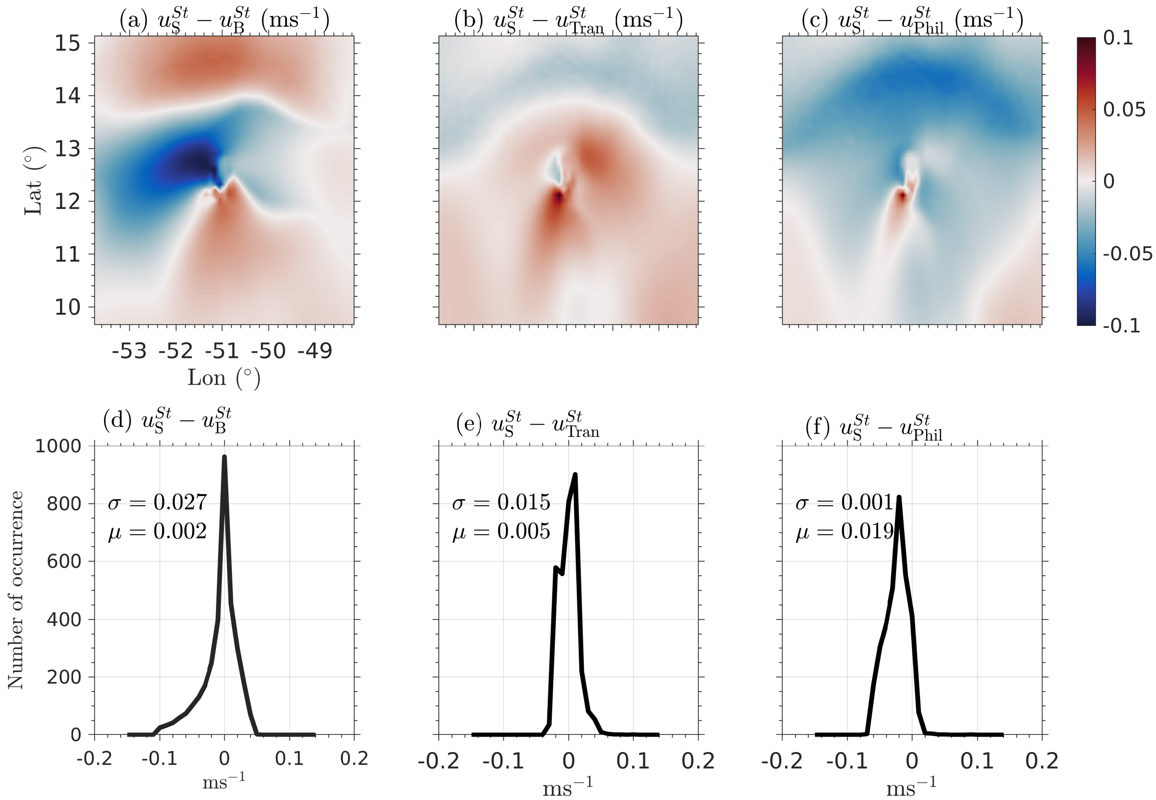

Figure 8. Color shading showing difference between near-surface Stokes drift magnitude U_S^{St} and U_B^{St} (a), U_{Tran}^{St} (b) and U_{Phil}^{St} (c) versus longitude and latitude. The probability distribution of differences corresponding to those shown in (a), (b) and (c), are reported in (d), (e) and (f), respectively, along with the mean and the standard deviation.

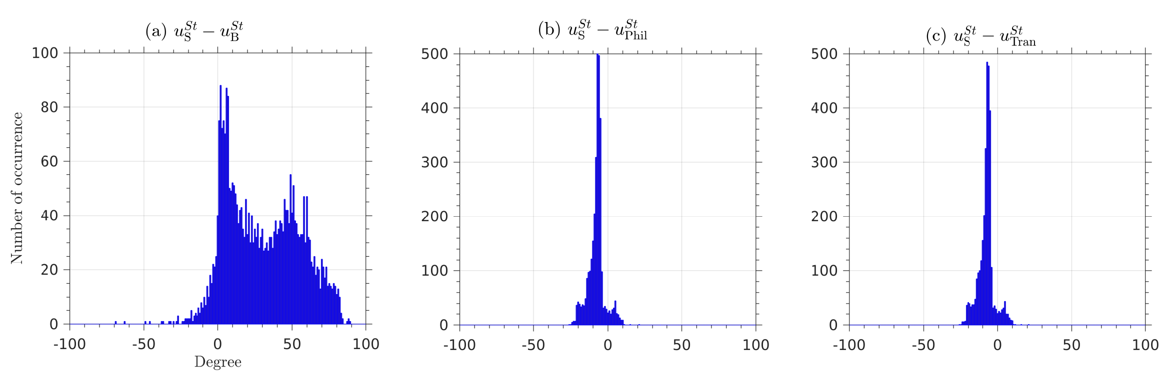

Figure 9. Probability distribution of difference between near-surface Stokes drift direction from u_S^{St} and u_B^{St} (a), u_{Tran}^{St} (b), and u_{Phil}^{St} (c).

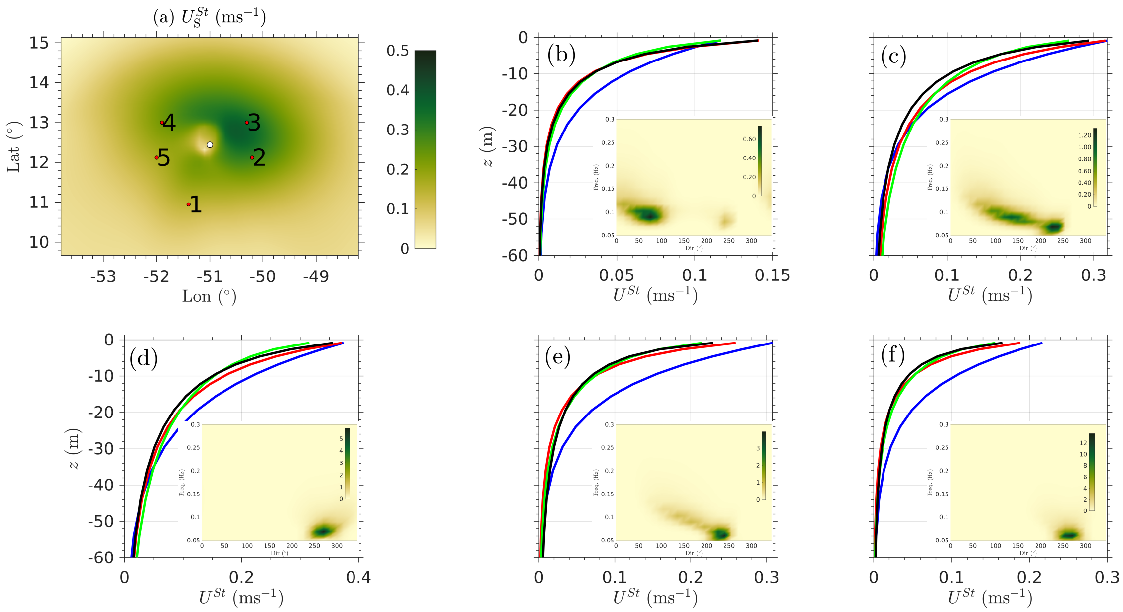

Figure 10. (a) Near-surface Stokes drift velocity magnitude $U^{\rm St}_{\rm S}$ versus longitude and latitude, along with selected points (1 to 5) at which the Stokes drift velocity magnitude profile and the frequency-directional wave spectra are shown. In b-f, the blue, black, green and red lines denote $U^{\rm St}_{\rm B}$, $U^{\rm St}_{\rm S}$, $U^{\rm St}_{\rm Phil}$ and $U^{\rm St}_{\rm Tran}$, respectively.

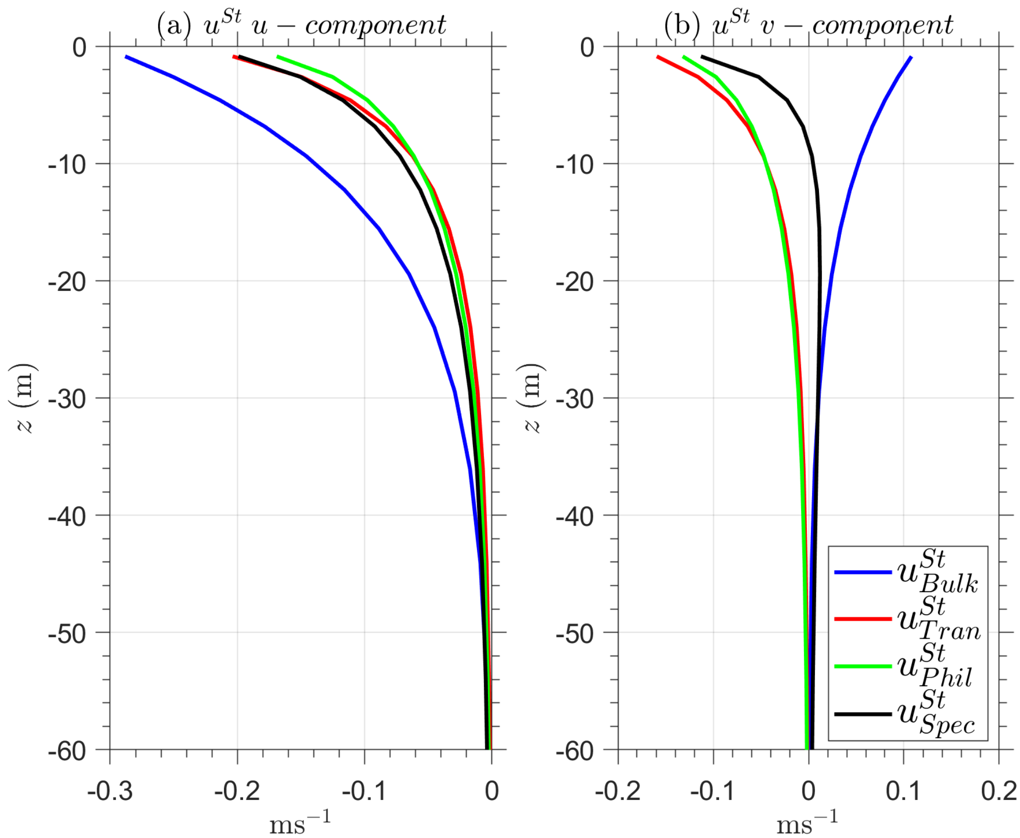

Figure 11. (a) Zonal and (b) meridional component of Stokes drift velocity profile at point 4. The blue, black, green and red lines in (a) denote the zonal components $u^{\mathrm{St}}_{\mathrm{B}}$, $u^{\mathrm{St}}_{\mathrm{S}}$, $u^{\mathrm{St}}_{\mathrm{Tran}}$ and $u^{\mathrm{St}}_{\mathrm{Phil}}$, respectively, and similarly the meridional components in (b).

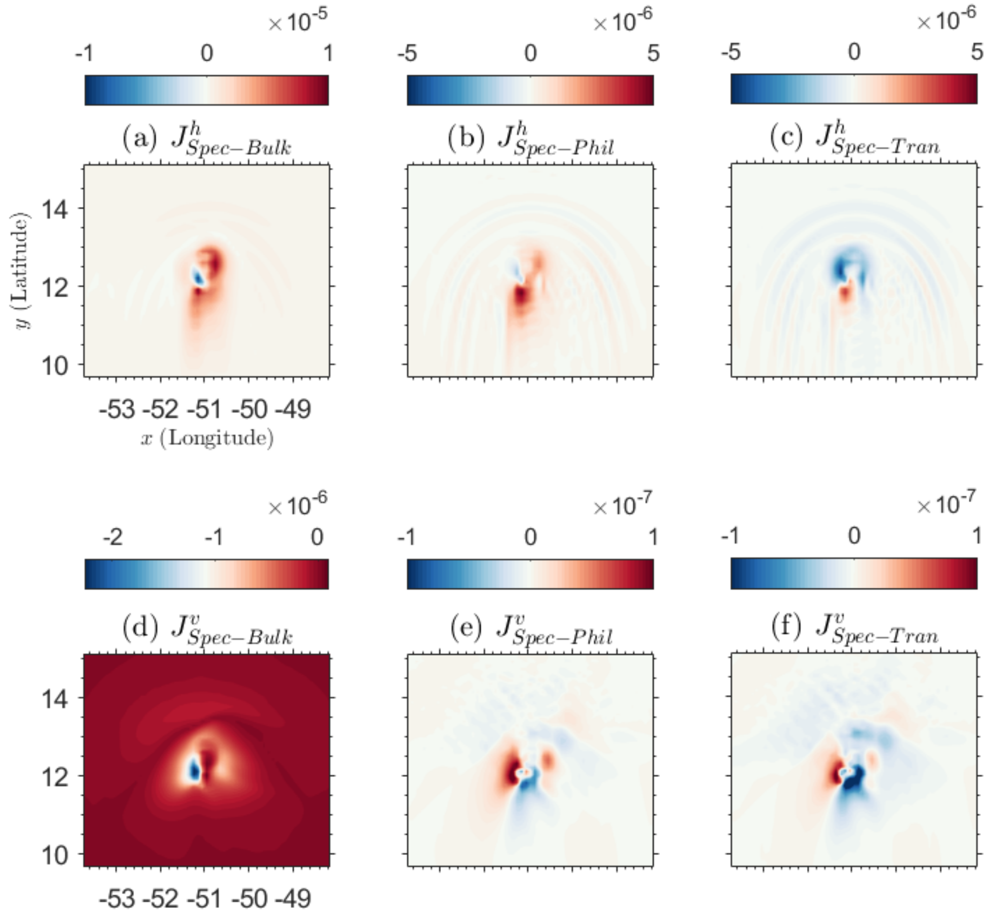

Figure 12. Differences of the horizontal (J^h) and vertical (J^v) vortex force components between u^{St}_{Spec} with other three methods. (a) Spatial difference of the J^h between u^{St}_{Spec} and u^{St}_{Bulk} methods. (b) Spatial difference of the J^h between u^{St}_{Spec} and u^{St}_{Phil} methods. (c) Spatial difference of theJ^h between u^{St}_{Spec} and u^{St}_{Tran} methods. (d)Spatial difference of the J^v between u^{St}_{Spec} and u^{St}_{Bulk} methods. (e) Spatial difference of the J^v between u^{St}_{Spec} and u^{St}_{Phil} methods. (f) Spatial difference of the J^v between u^{St}_{Spec} and u^{St}_{Tran} methods.(unit: ms^{-2})

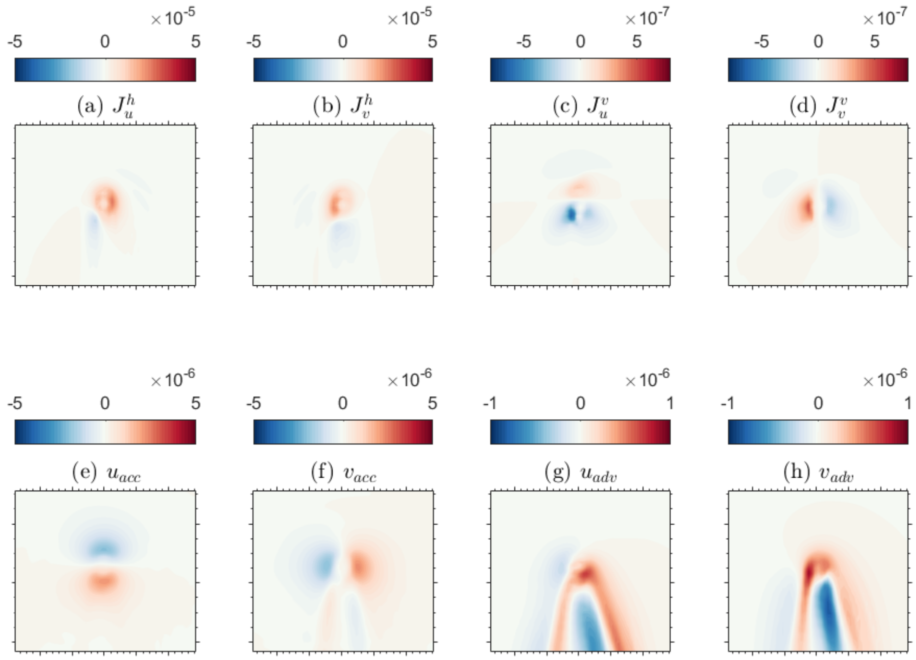

Figure 13. Distribution of horizontal vortex force (a) J_u^h, (b) J_v^h, (c) J_u^v, (d)J_v^v; the barotropic acceleration (e)u_{acc} , (f)v_{acc} , and the barotropic advection (g)u_{acc} , (h)v_{acc}.

Table 1. Model parameters for tidal inlet case

Model parameter	Variable	Values
Length, width, depth	Xsize, Esize, depth	15000 m, 14000 m, 4.0-14.7 m
Number of grid spacings	Lm, Mm, Nm	75, 70, 30
Bottom roughness	Z_{ob}	0.015 m
Time step	dt	10 s
Simulation steps	Ntimes	720 (12 hours)
Northern edge tide	Amp, T_t	1.0 m, 12 h
Northern edge wave height	H_s	1m
Northern edge wave period	T	10 s
SWAN time step	T_s	120 s

Table 2. Computational Cost

Methods	u^{St}_{Bulk}	u^{St}_{Tran}	u^{St}_{Phil}	u^{St}_{Spec}
Time	7 min 14 seconds	7 min 25 seconds	7 min 25 seconds	7 min 30 seconds